IRIS AperTO

UNIVERSITÀ DEGLI STUDI DI TORINO

AperTO - Archivio Istituzionale Open Access dell'Università di Torino

Advanced X-ray Absorption Spectroscopy Analysis to Determine Structure-Activity Relationships for Cu-Zeolites in the Direct Conversion of Methane to Methanol

This is the author's manuscript

Original Citation:

Availability:

This version is available http://hdl.handle.net/2318/1769038 since 2021-01-25T20:12:54Z

Published version:

DOI:10.1002/cctc.201902371

Terms of use:

Open Access

Anyone can freely access the full text of works made available as "Open Access". Works made available under a Creative Commons license can be used according to the terms and conditions of said license. Use of all other works requires consent of the right holder (author or publisher) if not exempted from copyright protection by the applicable law.

(Article begins on next page)

14 November 2026

IRIS AperTO

UNIVERSITÀ DEGLI STUDI DI TORINO

This is the author's final version of the contribution published as:

Kvande K.; Pappas D.K.; Borfecchia E.; Lomachenko K.A., Advanced X-ray Absorption Spectroscopy Analysis to Determine Structure-Activity Relationships for Cu-Zeolites in the Direct Conversion of Methane to Methanol.

CHEMCATCHEM, 12, 2020, 2385-2405.

DOI: 10.1002/cctc.201902371

The publisher's version is available at:

https://chemistry-europe.onlinelibrary.wiley.com/doi/abs/10.1002/cctc.201902371

When citing, please refer to the published version.

Link to this full text:

http://hdl.handle.net/2318/1769038

iris-AperTO

University of Turin's Institutional Research Information System and Open Access Institutional Repository

Advanced X-ray absorption spectroscopy analysis to determine structure-activity relationships for Cu-zeolites in the direct conversion of methane to methanol

Karoline Kvande,[a] Dr. Dimitrios K. Pappas,[a] Dr. Elisa Borfecchia[b] and Dr. Kirill A. Lomachenko*[c]

[a] Centre for Materials Science and Nanotechnology, Department of Chemistry, University of Oslo, Sem Sælands vei 26, 0371 Oslo (Norway)

[b] Department of Chemistry and INSTM Reference Center and Department of Physics, University of Turin, 10125 Turin (Italy)

[c] European Synchrotron Radiation Facility, 71 avenue de Martyrs, CS 40220, 38043 Grenoble Cedex 9 (France)

** kirill.lomachenko@esrf.fr*

Frontispiece

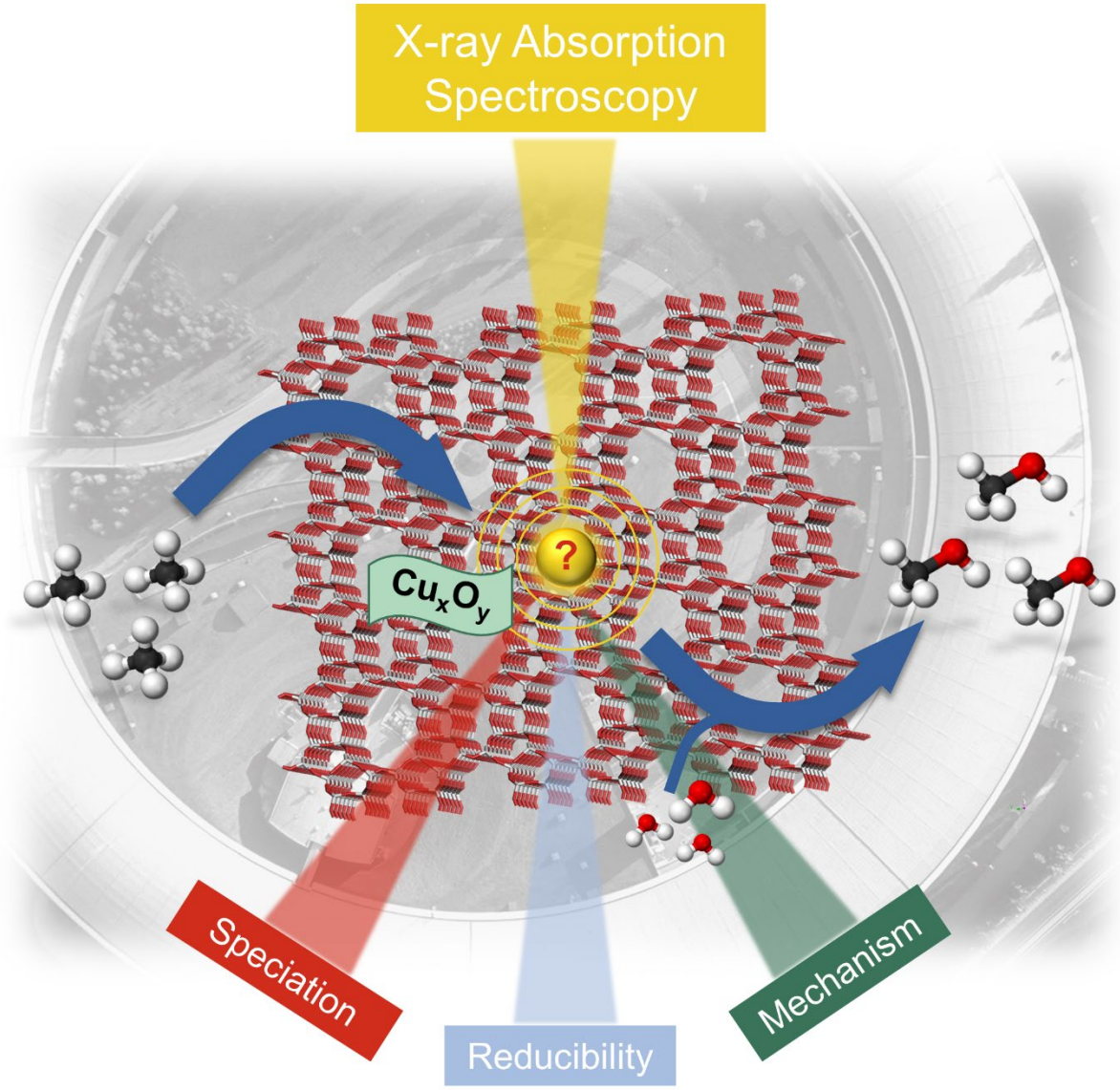

TOC picture

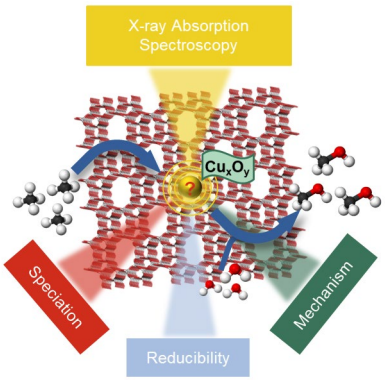

TOC description

X-ray absorption spectroscopy (XAS) is a powerful technique for investigating the active sites of nanoporous catalysts by following their structural and electronic changes under *in situ* and *operando* conditions. This review summarizes the recent XAS studies that focus on the speciation and reducibility of Cu centers in Cu-exchanged zeolites, providing mechanistic insights for the direct conversion of methane to methanol.

Abstract

An industrial process for direct conversion of methane to methanol (DMTM) would revolutionize methane as feedstock for the chemical industry and it would be a cherished contribution to climate change mitigation. At the present stage, it is a rather remote perspective, but the search for the materials that would make it possible and economically viable, is very active. Cu-exchanged zeolites have been shown to cleave the C-H bond of methane at low temperatures (≤ 200 °C), and has been extensively studied for the stepwise DMTM conversion over the last decades. The determination of the speciation of Cu_xO_Y-species in zeolites and understanding their role in the reaction mechanism has been heavily debated. Lately, advanced X-ray absorption spectroscopy (XAS) analysis has been standing out as a powerful technique for investigating the behavior of Cu in the zeolite. In this review we focus on the *in situ* and *operando* studies of the changes in the electronic and structural properties of Cu during the different steps of the DMTM conversion uncovered by XAS, which have led to new and insightful information about the complex behavior of Cu-zeolites in the DMTM process.

Biographies

Karoline Kvande is a PhD candidate at the Department of Chemistry at the University of Oslo. Her project involves investigating the direct activation of lower alkanes over transition metal containing materials. The work is in collaboration with Haldor Topsøe. From before, she holds an MSc on the same topic from the University of Oslo. Over the course of her studies, she has been working extensively with activity testing, as well as working on a wide range of characterization techniques suitable for investigating metal-loaded materials.

Dr. Dimitrios Pappas obtained his PhD in Chemistry in 2019 from the University of Oslo (Norway). His research focused on establishing structure-activity relationships for the direct conversion of methane to methanol over Cu-exchanged zeolites by combining activity measurements and mainly X-ray absorption spectroscopy. He has also worked on the selective catalytic reduction of NOx and soot oxidation during his MSc at University of Cincinnati (USA) and Diploma in chemical engineering at Aristotle University of Thessaloniki (Greece) respectively. Currently he is a research scientist at CoorsTek Membrane Sciences (Norway)

Dr. Elisa Borfecchia received her PhD in Science and Technology of Materials in 2013 at the University of Turin (Italy). Through the following fellowships at Universities of Turin and Oslo and in Haldor Topsøe, her research activity has focused on the application of synchrotron techniques to the characterization of catalysts. As a researcher at the University of Turin, today she pursues the integration of in situ/operando X-ray spectroscopy with laboratory techniques and modelling to unravel the reactivity of redox-active metal ions in microporous materials.

Dr. Kirill A. Lomachenko obtained his PhD in Chemistry and Materials Science in 2016 pursuing a joint PhD program between University of Turin (Italy) and Southern Federal University (Russia). His research is focused on the in situ and operando investigation of coordination environment and electronic structure of active sites in various types of modern catalysts, such as metal-organic frameworks, zeolites and supported nanoparticles by X-ray absorption spectroscopy and complementary techniques. Being currently a beamline scientist at ID24 and BM23 XAS beamlines at the ESRF, he is also in charge of developing instrumentation for synchrotron-based XAS studies in the field of heterogeneous catalysis.

1. Direct CH_4 to CH_3OH Conversion over Zeolites

Over the last decades, methane has become more available through the production of natural gas. As a direct consequence of that, more and more literature is found on the direct methane to methanol (DMTM) conversion. Methane is a potent greenhouse gas, and since it also is an abundant energy source, there is an increasing interest in finding good solutions for converting CH_4 to more high-value products. The industrial method for converting CH_4 today is the production of synthesis gas (CO, H_2), which is then converted further into other products, such as olefins, alcohols and ethers.[1] This process requires large production facilities, since the economic benefits directly correlate with the capacity of the production site. At remote areas, such as oilrigs, natural gas extracted with the oil is usually flared, releasing more than 300 million tons of CO_2 to the atmosphere annually.[2] The direct conversion of CH_4 to a liquid product, such as CH_3OH, has therefore received an increasing interest in academia and industry as a step further on our route to a more sustainable environment. Since CH_4 is a very stable molecule, one of the most pressing tasks is to find a reaction process that prevents over-oxidation. Cu-exchanged zeolites have proven to be possible candidates for such process.[3] Nevertheless, determining the nature and mechanism of the active Cu_xO_y species has proven to be difficult, and numerous techniques have been employed in order to understand more about the active sites. This review will summarize the recent results on the use of X-ray absorption spectroscopy (XAS) on Cu-zeolites for the DMTM. We will illustrate the versatility and the potential of this technique, which is likely to become one of the most important tools for completely unraveling the nature of the active sites in DMTM.

1.1. CH_4 Activation over TM-Exchanged Zeolites

Zeolites are microporous aluminosilicates with defined structures built from tetrahedral TO_4 units (T = Al, Si). Zeolites are open microporous structures consisting of channels and cavities. They are classified based on the pore size (small, medium and large), the dimensionality of their channel system (0D, 1D, 2D and 3D) as well as other structural features.[4] Zeolites are used as commercial catalysts in fluid catalytic cracking (FCC) and hydro cracking (HC) while

other applications include alkylation, isomerization, cumene production, selective catalytic reduction of NO_x and reforming. The ion exchange properties of zeolites, their well-defined structure, high internal surface area and microporosity make them attractive materials for catalysis. The fact that zeolites have channel sizes of molecular dimensions introduces shape selectivity in the framework, which combined with Brønsted acidity, has led to the commercialization of zeolites as catalysts in the methanol-to-hydrocarbons (MTH) reaction for the production of olefins, gasoline and aromatics.[5] Negative charge of the framework can be compensated by different metal cations like alkaline metals, transition metals or cationic metal complexes hosted in the zeolitic cavities, which gives rise to active metal centers and thus enhances the functionality of the material.

Different TMs, besides Cu, have been employed for DMTM conversion including: Fe,[6] Co,[7] Ni,[8] Rh,[9] Zn.[10] The DMTM conversion over TM-exchanged and especially Cu-exchanged zeolites deviates from a steady state catalytic process, since it is frequently carried out in a stepwise fashion avoiding mixing CH_4 with O_2 in order to prevent overoxidation and maintain high CH_3OH selectivity.

In the early 1990s, Panov and coworkers identified α-oxygen species formed upon decomposition of N_2O over alpha-Iron (a-Fe) in Fe-ZSM-5, which constitutes part of the site active for DMTM conversion at room temperature with 80 % selectivity.[6f, 11] Based on combined spectroscopic and computational findings, the Fe active site in ZSM-5 as well as in BEA has been proposed to be high-spin Fe^{II} center located in beta-type 6-membered ring (MR) with a square planar geometry.[12] Panov et al. studied the reaction in a quasicatalytic fashion initially co-feeding CH_4 and N_2O at 160 °C over the O_2-activated sample at 550 °C ultimately yielding 160 μmol/g of CH_3OH and 49 μmol/g of CH_3OCH_3.[6g]

Hammond *et al.* studied the efficiency of a stronger oxidant (i.e. H_2O_2) to activate the Fe-ZMS-5 establishing the DMTM conversion in liquid phase.[6b-d] The CH_4 activation energy for this system was calculated to be 14.6 kcal/mol, while promoters such as Cu were utilized to improve the selectivity towards oxygenates.[6b-d] The active sites after activation by H_2O_2 in liquid phase have been shown to be binuclear Fe^{III} species and their structure was confirmed to be $[Fe_2(\mu\text{-}OH)_2(OH)_2(H_2O)_2]^{2+}$ based on density functional theory (DFT) calculations complemented by extended X-ray absorption fine structure (EXAFS) fitting.[6b] The Cu-

promoted Fe-ZSM-5 tested in batch[6b] and flow[13] reactors exhibited 0.7 and 0.5 CH_4 conversion (%) as well as 85 and 92 CH_3OH selectivity (%) respectively. However, the price of H_2O_2 as well as the CH_3OH extraction pose limitations to such systems.[14]

Co-ZSM-5 (MFI framework topology) has also been reported to possess activity for the DMTM conversion at 150 °C, after O_2 activation at 550 °C, obtaining 0.4 μmol/g_{cat} of CH_3OH following a stepwise reaction mode.[7a] Co^{II} populates three different exchange sites in the MFI framework, although the exact location, geometric and electronic structure of the Co active site is not yet fully resolved.[15] Likewise, Ni-exchanged zeolites (Ni-ZSM-5) require high-temperature O_2 activation (600 °C) in order to obtain active Ni moieties, identified as $[Ni_2(\mu\text{-}O)]^{2+}$ using ultraviolet-visible spectroscopy (UV-vis) and EXAFS fitting.[8]

Zn-modified zeolites were initially studied for CH_4 aromatization; later Stepanov and co-workers discovered their ability to activate the C-H bond in CH_4 at low temperatures.[10a, 10b, 16] The active Zn site has been shown by Gabrienko *et al.* to consist of isolated Zn^{II} species, opposed to ZnO for benzene alkylation with CH_4.[10b] Very recently, Oda *et al.* combined spectroscopic and theoretical results to identify Zn−oxyl species (Zn^{II}-$O^{\bullet}$) in MFI as the active species for CH_4 activation at RT; while Zn-OCH_3 was observed by Infrared spectroscopy (IR) as the reaction intermediate.[10c]

Cu-exchanged zeolites are probably the most studied zeolites in the field of DMTM conversion, because they are considered the most promising for industrial application.[3c, 17] Just as Fe, Cu is believed to form the active sites in methane monooxygenase (MMO), which is an enzyme able to convert CH_4 to CH_3OH at ambient conditions with a high selectivity. Cu forms the active sites in the particulate form (pMMO) and Fe in the soluble form (sMMO).[18] However, unlike Fe, both O_2 and N_2O can be used to activate Cu, making Cu-zeolites much more preferable for industrial applications. The use of Cu-zeolites for DMTM has provided the highest yields thus far and will therefore be the sole focus of this review.

1.2. Cu-Exchanged Zeolites

From the early 1980s Cu-Y and later Cu-ZSM-5 among other zeolites were investigated by Iwamoto *et al.* for the decomposition of NO, exhibiting stable and high activities.[19] After this

discovery, Cu-exchanged zeolites were an object of continuous research as catalysts for NO decomposition[20] as well as for the hydrocarbon- and NH_3-assisted selective catalytic reduction of nitrogen oxides (HC- or NH_3-SCR of NO_x).[21] However, the application of medium- and large-pore Cu-exchanged zeolites in NH_3-SCR was inhibited by the lack of low temperature activity, fast deactivation and excessive NH_3 storage.[21c, 22] Cu-exchanged small pore zeolites and zeotypes, with CHA topology (Cu-SSZ-13 and Cu-SAPO-34 respectively), assisted in resolving the aforementioned issues and were commercialized as NH_3-SCR of NO_x catalysts in 2009.[21c] A substantial amount of research has been devoted into studying Cu-CHA catalysts, focusing on the SCR reaction mechanism, Cu speciation, their low temperature SCR activity as well as their hydrothermal stability.[23] Beyond NH_3-SCR, Cu-exchanged zeolites are active for the oxidation/hydroxylation of benzene to phenol,[24] and last, the activation of CH_4 and its subsequent transformation to CH_3OH, which is the focus of this review.

The most common method to exchange Cu ions in the zeolitic framework is liquid ion exchange (LIE), where the cations in the zeolite (H^+, Na^+ and NH_4^+) are exchanged in solution with Cu; the most common Cu^{II} complex in solution is $[Cu(H_2O)_6]^{2+}$. Different parameters affect the synthesis, such as the zeolite structure, the Cu precursor and the pH, which has been identified to be very important and must be adjusted below six (pH < 6) to avoid Cu precipitation.[3e, 25] The exchange can also be achieved by solid state ion exchange (SSIE) or incipient wetness impregnation. This involves heating of the zeolite along with a Cu precursor (usually $CuCl_2$). Depending on whether the parent zeolite is in the H- or Na-from, HCl or NaCl are produced during heating. After the synthesis, the sample is activated/calcinated to remove H_2O as well as organic/inorganic residues from the synthesis. Successively Cu coordinates to lattice oxygen of the framework.[25a] The location, electronic state and geometrical configuration of Cu ions in the zeolite depends on the framework topology. Currently among the most studied zeolites for DMTM process are Cu-exchanged CHA, FER, MOR, FAU and MAZ materials. The frameworks of these zeolites are presented in Figure 1.1, whereas the overview of their structural units is given in the Table 1.1.

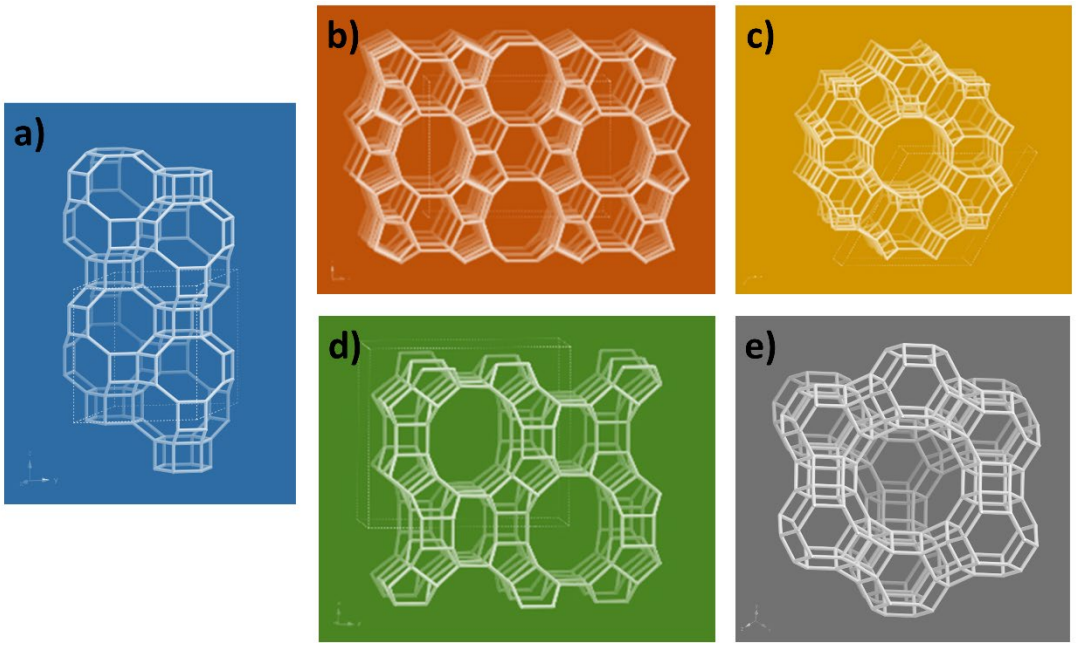

Figure 1.1 Illustration of the zeolite frameworks presented in this review; (a) CHA, (b) FER, (c) MAZ, (d) MOR and (e) FAU.

Table 1.1 Structural characteristics of selected zeolite framework types

FRAMEWORK	RING SIZES	CHANNEL DIMENSIONS (Å)	CHANNEL GEOMETRY	UNIQUE T-SITES	NO. OF PROPOSED Cu EXCHANGE SITES
CHA	8MR/6MR/4MR	8MR channel (3.8x3.8)	3D	1	4
FER	10MR/8MR/6MR/ 5MR	10MR channel (4.2x5.4) 8MR channel (3.5x4.8)	2D	4	3
MOR	12MR/8MR/5MR/ 4MR	12MR channel (6.5x7.0) 8MR channel (2.6x5.7)	1D	4	3-5
FAU	12MR/6MR/4MR	12MR channel (7.4x7.4)	3D	1	6
MAZ	12MR/8MR/6MR/ 5MR/4MR	12MR channel (7.4x7.4) 8MR channel, distorted (3.1x3.1) 8MR channel (3.9x3.9)	1D	2	1-2

* d = diameter

The habazite (CHA) topology is a symmetric framework of cages constructed from two 6MR, six 8MR and twelve 4MR, with the latter interconnecting the rest; the entrance to the cages is through the 3.8 x 3.8 Å opening of the 8MR. Cu-SSZ-13 was initially proposed to have a sole Cu configuration placing the cation in the 6MR.[23e, 26] Conversely, later reports present a more complex picture, concluding the existence of multiple docking sites for Cu in the 6MR and 8MR.[23a, 23o, 27] The resulting nature of Cu species is a combination of multiple factors including the composition (Si/Al and Cu/Al ratios) as well as the temperature and the gaseous environment (oxidative and reductive) under which the material is investigated.[3h, 23a, 23o, 23u,

[27a, 28] The aforementioned factors influencing the speciation can be considered relevant for most Cu-zeolites.

The Ferrierite (FER) structure is a 2D channel structure. The framework is composed of 10MR channels (5.4 x 4.2 Å, along the [001] direction) intersected by 8MR channels (4.8 x 3.5 Å, running along the [010] direction) and 6MR channels in the [001] direction; the FER contains 4 different T-sites accessible from the 10MR. Similar to CHA, FER has been proposed to possess multiple cationic sites defined as α-, β- and γ-sites by Wichterlová and coworkers.[15b, 29] This expands the initial proposal of a single site at the channel intersection of the 10MR and 8MR.[30] The α-site is a planar 6MR along the straight channel with an O-T-O bridge while, the β-site is a planar 6MR in the perpendicular channel. These sites have also been identified in the MFI framework.[31] The γ-site is boat-shaped with one O-T-O bridge and is found in the intersection of the straight and perpendicular channels. Cu^{I} species have been identified to populate all three sites,[29b-d, 32] and the binding energy of these species in the walls of the channels (α- and β-site) has been found to be lower compared to the one at the intersection (γ-site).[29d] The location of Cu^{II} ions on the other hand, was studied experimentally by synchrotron XRD, electron spin resonance spectroscopy (ESR)[30] as well as DFT calculations.[32] Initially, the intersection of the two channels (γ-site) has been proposed as a site for weakly coordinated Cu^{2+} ions highly accessible to reactants.[30] $[Cu(H_2O)_6]^{2+}$ species observed by ESR, in the main channel or at the center of the cage, were suggested to be the precursors to the framework-interacting Cu^{II} species upon full dehydration at 360 °C.[30] Later Sklenak *et al.* located Cu^{II} ions in the 6MR in the wall of the main 10MR channel as well as in the deformed 6MR in the perpendicular 8MR channel.[32] Depending on the Al siting, the 8MR channel site was reported to be preferentially populated due to a higher Cu^{II} binding energy, compared to the one in the main channel, making the latter more reactive.[32]

The mordenite (MOR) topology consists of straight 12MR channels with a diameter of 7.0 × 6.5 Å and perpendicular 8MR side pockets with a diameter of 5.7 × 2.6 Å (Figure 1.1). The research on Cu speciation in MOR started in 1992 with Kuroda *et al.* reporting Cu divalent ions in the MOR with tetragonal symmetry, which form dimeric species based on different spectroscopies (EPR, IR, EXAFS and XANES).[33] Later, three distinct Cu^{II} locations have been identified by Attfield *et al.,* based on XRD and ESR. These include the elliptical 8MR, the 6MR

adjacent to the 8MR channel and the 8MR adjacent to the 12MR (later referred as the 8MR side pocket) with the last two being more accessible to reactants. Vanelderen *et al.* also identified three Cu^{II} species for O_2-activated Cu-MOR; two of them were isolated ions while the third was tentatively assigned to a binuclear copper site. The latter species were reported to be reduced upon heating in hydrogen at 180 °C.[34] Subsequently, the same group suggested two sites in the 8MR (inside the 8MR channel and 8MR window adjacent to the 12MR main channel), which can host the $[Cu(\mu\text{-}O)Cu]^{2+}$ with different reactivity.[35] Snyder *et al.* studied the second sphere effects on the reactivity of the two $[Cu(\mu\text{-}O)Cu]^{2+}$ found in the 8MR using Raman and DFT.[36] Despite similar geometric and electronic structures, the reactivity towards CH_4 was found to be higher for the more constricted site (inside the 8MR).[36]

The FAU zeolite has a diamond like array and is built up of sodalite cages interconnected with double 6MR. 10 sodalite cages make up the inner cavity, a supercage, which has a diameter of 12 Å.[37] The pores of the FAU zeolite are made up of 12MR and are 7.4 Å in diameter. Depending on the Si/Al ratio, FAU is also known as zeolite-X (Si/Al ~ 1.0 – 1.4) or –Y (Si/Al ~ 1.5 – 3.0).[38] Six Cu exchange sites have been shown by crystallography to exist inside the FAU framework. One is inside the double 6MR (I), one at the interface between the double 6MR and sodalite cage(I'), then three are connected with the 6MR of the sodalite cage facing towards the supercage (II, II' and II*), and last one near the center of a 12MR (III), between two supercages.[39],[40] In 1959, Zeolite Y was used as the first industrial catalyst and functioned as an isomerization catalyst for Union Carbide.[41] Since then, FAU zeolites have been heavily investigated as catalyst for various industrial processes, such as oxidation, cracking and isomerization reactions.[42] The nature of the cation and Cu ion sites in FAU zeolites have been extensively studied over the years. Cu ions situated inside the double 6MR or in the sodalite cage are less likely to function as active sites. This is due to the 6MR entrance of the sodalite cage being too narrow for molecules to diffuse through (free diameter ~0.23 nm).[43] On this basis, it is believed that the active Cu-sites are situated inside the supercage (site II* and III). Although, it should be noted that Cu situated inside the sodalite cage have been observed to migrate towards the supercage in certain atmospheres, such as in the presence of CO.[44]

The mazzite (MAZ) topology is made up of columns of gmelinite cages (structural units typical also for gmelinite zeolite with GME topology), with its 6MR windows facing the [001] direction.

The cages are interconnected with an O-bridge, forming 12MR channels through the zeolite with a diameter of about 8 Å. 8MR pores are formed from interconnected gmelinite cages and forms a third set of channels parallel to the 12MR pore.[45] These channels have a free diameter of 3.4 x 5.6 Å. Last, there is a somewhat distorted channel moving perpendicular to the [001] direction formed from the 8MR window of the gmelinite cages. This channel system is inaccessible from the 12MR channel.[46] It is also showed that the access to the column of gmelinite cages is very restricted due to complicated diffusion paths.[47] It has been shown that MAZ has two non-equivalent crystallographic sites (T1 and T2).[48] The T2 site, suggested to be a very strong Brønsted acidic sites (BAS), is situated in the 12MR, and the T1 site is in the intersection between the 8MR and 6MR of the gmelinite.[49] T1 has, however, been shown by ^{29}Si and ^{27}Al MAS NMR to be the preferred location for Al atoms.[50] In an early study based on ESR, it was suggested that hydrated Cu^{II} exists in the 12MR main channel coordinated to three water molecules and framework O. Upon dehydration, the Cu migrates to the 6MR window of the gmelinite cage. Further, it is implied that the back migration of Cu^{II} to the main channel is restricted, leading to the observation that only small molecules, able to diffuse into the gmelinite cages, are able to coordinate to the Cu ions.[46]

1.3. DMTM Conversion Over Cu-Exchanged Zeolites

Groothaert *et al.* in 2005 demonstrated the ability of Cu-oxo centers in Cu-containing zeolites (Cu-MOR and Cu-ZSM-5) to activate the C-H bond of CH_4 and transform it to oxygenates via dissolution.[3b] The active site, identified at that time as a bis(μ-oxo)dicopper ($[Cu(\mu\text{-}O)_2Cu]^{2+}$), was able to cleave the C-H bond and stabilize the intermediate at 175 °C, which was then extracted as CH_3OH in a 1:1 water/acetonitrile solution (98 % selectivity).[3b] These early findings suggested a stepwise conversion of CH_4 to CH_3OH over Cu-exchanged zeolites. The process consists of three steps, as shown in Scheme 1.1. The material is first activated at high temperature (450 °C) in presence of an oxidant (usually O_2). Then, the material is reacted with CH_4 at lower temperatures from 60 to 200 °C and finally CH_3OH is extracted using solvents, with ethanol and acetonitrile/water being the most efficient,[51] or by online extraction passing steam through the reactor (Scheme 1.1).[3d]

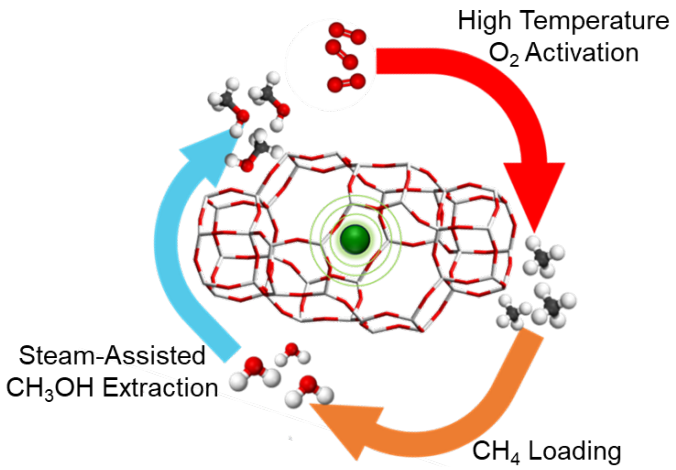

Scheme 1.1. Pictorial representation of the sequential steps involved in the DMTM conversion over Cu-exchanged zeolites.

In one of the first studies (2005), Smeets *et al.* screened a wide set of Cu-exchanged zeolite structures including MFI, MOR, EMT, FER, BEA, FAU as well as SiO_2 and Al_2O_3 for the DMTM conversion.[52] Up to date, numerous zeolites have been shown experimentally to be active for the DMTM conversion. Among them, Cu-MOR,[3b-e, 3g, 25b, 35, 53] Cu-ZSM-5,[3a, 3b, 3f, 51-52, 54] Cu-SSZ-13,[3h, 3i, 28, 53e, 53f, 54e, 55] Cu-MAZ,[53e, 56] and Cu-FER.[52, 53e, 53h, 54e] Besides Cu-exchanged zeolites, CuO/SBA-15,[57] Cu-SiO_2[58] and Cu-Al_2O_3[59] have also been investigated for DMTM process. After the provided overview on the process conditions and on the different zeolites active for DMTM, a more detailed look into the individual steps constituting the DMTM conversion follows.

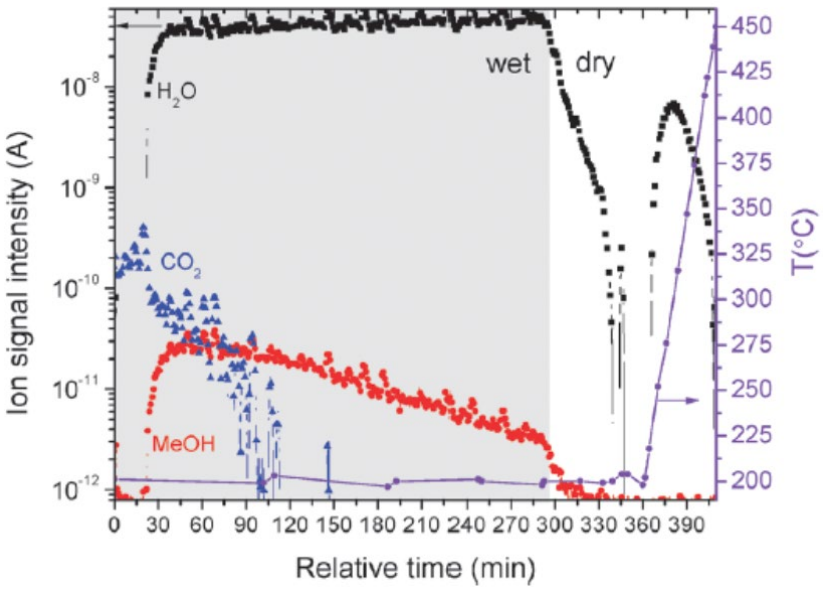

Scheme 1.1. First demonstration in literature of online CH_3OH extraction with steam by Alayon et al.[3d] Mass spectrometer-detected signals of H_2O(m/z = 18), CO_2 (m/z = 44) and CH_3OH (m/z = 31) during the treatment with wet He at 200 °C after CH_4 interaction, and the subsequent heating in dry He at 5 °C/min. Adapted from Alayon et al. [3d]

1.3.1. Activation

High temperature oxidative treatment is the first step of the cyclic DMTM conversion. The Cu-exchanged zeolites are activated at high temperatures, 400 – 500 °C, usually in an O_2-containing atmosphere. Thermal treatment at high temperature removes H_2O and organic residues from the synthesis, while it results in Cu ions coordinating to the framework to compensate for the negative charge.[36]

The O_2 activation temperature has been suggested in several studies as a parameter that can affect the CH_3OH yield.[3i, 28, 52, 53e, 53h, 53i, 60] As a general trend, low temperature below 300 °C does not enable the population of active sites, subsequently resulting in lower activity. On the other hand, temperatures above 550 °C have shown to result in Cu aggregates, which have been reported to be inactive or unselective.[53e] Park *et al.* studied the effect of activation temperature from 200 to 550 °C and its impact on CH_3OH productivity over a variety of Cu-exchanged zeolites (MOR, ECR, MAZ, PST, UZM). Most materials exhibited a volcano like behavior with a peak at 450 °C.[53e] Non-zeolite materials, such as Cu-SiO_2 and Cu-Al_2O_3 require higher temperatures in the 700 – 800 °C range to obtain yields comparable to Cu-zeolite systems.[58-59]

On the other hand, He activation of Cu-SSZ-13 has been reported by Oord *et al.*[55b] to decrease the CH_3OH yield. This is in contrast to results from Ipek *et al.*[28] for Cu-SSZ-13 and Brezicki *et al.*[25b] for Cu-MOR, both reporting substantial CH_3OH yields, even in the absence of an oxidant. Ipek *et al.* attributed this activity to self-reduction resistant multimeric Cu-oxo species,[28] while Brezicki *et al.* attributed it to ppm levels of O_2 impurities.[25b] Decoupling dehydration/self-reduction from O_2/N_2O activation, Ikuno *et al.* signified the importance of He activation temperature, with 500 °C being more efficient than 350 °C, prior to reoxidation of Cu-MOR with respect to the CH_3OH yield.[53j] Different reoxidation temperatures (50 - 200 °C) of a pre-reduced Cu-MOR at 500 °C, with either O_2 or N_2O, yielded comparable CH_3OH amounts.[53j]

It is evident that O_2 and air are the preferred oxidants, because they are more industrially pertinent. Albeit, NO,[54a] N_2O[54a, 60-61] and even H_2O[3c, 53c] have been demonstrated to generate Cu-oxo species. N_2O activation of Cu-MOR and Cu-ZSM-5 has been reported to be effective only for low Cu-Cu (<4.2 Å) distances allowing O bridging.[35] Kim *et al.* compared N_2O and O_2 activation of Cu-MOR showing that N_2O is more efficient at low (300 – 350 °C) and high (500 – 600 °C) temperatures .[60] Conversely, Ikuno *et al.* did not observe differences when comparing the two oxidants for Cu-MOR zeolites in the 200 – 500 °C temperature range, even when decoupling dehydration and reoxidation.[53j] However, in the case of Cu-SSZ-13, Ipek *et al.* also suggested that N_2O is a more efficient oxidant at low temperatures.[55a]

Sushkevich *et al.* have investigated the anaerobic DMTM conversion over Cu-MOR; the samples were initially activated in He at 400 °C, followed by 7 bar CH_4 loading at 200 °C and finally the products were extracted online with steam yielding 0.142 molCH_3OH/molCu.[3c] The authors suggested that H_2O, during extraction, assists product desorption, while at the same time acting as a "soft" oxidant regenerating the active sites, and after the first cycle the sample yields 0.202 molCH_3OH/molCu with a selectivity of 97 %.[3c] However, for low Al-content (Si/Al = 46), the CH_3OH yield was very low, and it was suggested that H_2O is not able to activate monomeric Cu-sites.[53c] In addition, it is important to take into consideration the results from Brezicki *et al.* regarding the O_2 impurities in He feed reacting with a He-activated sample forming active sites. This is especially important at CH_4 reaction temperatures, where thermodynamics favor the adsorption of O_2 by Cu^I sites.[25b]

1.3.2. CH_4 Loading

Following activation, the temperature is lowered (100 – 300 °C) and CH_4 loading takes place. The cleavage of the C-H bond occurs over $[Cu_xO_y]^{2+}$ species, most likely through a radical rebound mechanism. Activation of CH_4 has been proposed, in early reports, as the rate limiting step of the cyclic process.[3a, 3b, 54b] A hypothetical reaction mechanism would involve the adsorption of CH_4 on the active site, followed by the homolytic bond cleavage via a radical-like transition state to form a methyl that later recombines with the OH in order to form CH_3OH bound on the site,[62] as presented in Scheme 1.2 together with other proposed radical and non-radical reaction pathways. The presence of BAS is suggested to be beneficial for the

yield and selectivity, since they can stabilize the reaction intermediate and prevent overoxidation.[53d] On the other hand, the presence of Na^+ or other alkali and alkaline earth cations results in the decreased activity, because they compete for the exchange positions preferred by Cu^{2+}.[3g] As a result, H-form zeolites outperform their Na-form analogues.[3g, 53d]

It is evident in the literature that prolonged contact time,[53i] as well as high CH_4 partial pressure,[3f, 25b, 63] assist the CH_3OH yield. In general, CH_4 activation occurs around 200 °C. This temperature has been reported to enhance the CH_3OH yield for Cu-MOR[52] and Cu-FER[52] compared to 150 °C, while in the case of Cu-ZSM-5 no effect was observed.[64]

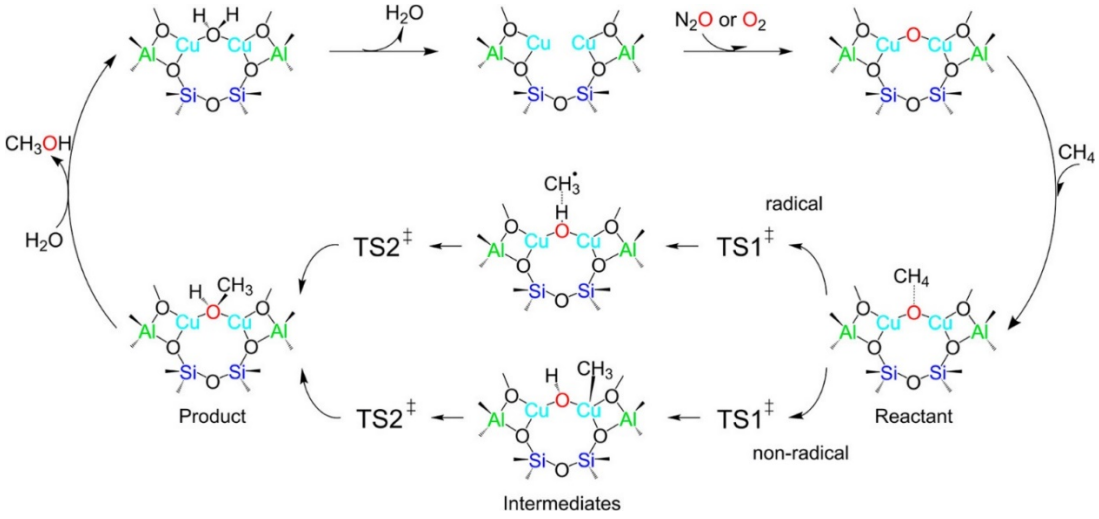

Scheme 1.2. Possible reaction pathways for CH_4 hydroxylation over $[Cu(\mu\text{-}O)Cu]^{2+}$ active site in zeolites, adapted from Mahyuddin et al. [65]

The zeolite framework has been theoretically suggested to assist the CH_4 dissociation through confinement. This can be attributed to the confinement of free space for interaction, between CH_4 and Cu-oxo species or by just assisting the stability and reactivity of the active sites.[54b, 66] As mentioned in Section 1.2 for Cu-MOR two locations for $[Cu(\mu\text{-}O)Cu]^{2+}$ have been proposed with different reactivity due to confinement effect.[35-36]

CH_4 pressure is shown to affect the CH_3OH yield.[3f, 25b, 63, 67] Tomkins *et al.* studied the effect of O_2 and CH_4 pressure on the isothermal DMTM conversion at 200 °C. High pressure of CH_4 increases the CH_3OH yield for Cu-MOR, reaching 56.2 µmol/g at 37 bar, while increasing O_2 pressure during the activation step has only a weak effect on performance, even leading to its marginal decrease.[3f] Similar results were also obtained for Cu-Y and Cu-ZSM-5.[67] Small dehydrated Cu clusters, less reactive than the well-defined dicopper sites, are suggested to

participate in the reaction at elevated CH_4 pressures.[3f] Recently Brezicki *et al.* compared the effect of CH_4 pressure after high temperature activation of Cu-MOR, showing ~30 % increase in the C_1 yield when CH_4 is loaded at 35 bar for 20 h, compared to 1 bar for the same time.[25b] For Cu-FAU it was shown that in the isothermal DMTM conversion at 360 °C a pressure increase from 1 to 15 bars results in a fourfold increment of the yield, leading to 360 μmol/g, the highest yield reported to date. [68] From a yield perspective, with the exception of Cu-FAU, the isothermal route at high CH_4 pressures compared to the high temperature activation route produces similar amounts of CH_3OH.[63] However, an isothermal operation would assist in eliminating large temperature swings associated to high operation costs, making it more attractive for industrialization.[69]

1.3.3. CH_3OH Extraction

After the stabilization of the intermediate, from the reaction between CH_4 and Cu-oxo species, the extraction of CH_3OH follows. In the early reports, CH_3OH was extracted by using solvents, resulting in very dilute CH_3OH solutions. Alayon *et al.* demonstrated that being introduced as a form of steam online (Scheme 1.1), H_2O is able to react with the adsorbed species and form CH_3OH, possibly by displacement via competitive adsorption.[3d] Different steam-assisted CH_3OH extraction temperatures can be observed in the literature. High temperature (around 200 °C) assists the yield[3h, 3i] by reducing the CH_3OH free energy desorption barrier[62] while slightly sacrificing the CH_3OH selectivity (%) due to overoxidation (CO_x). Lange *et al.* studied the effect of H_2O content in steam; their results show that high H_2O contents (18 %) facilitate a faster desorption, reducing the desorption time by ~2 h, compared to 2.8 % H_2O.[69]. On the other hand, excessive steam also leads to a very dilute CH_3OH stream, necessitating separation as well as restoration of the hydrolyzed Cu_xO_y.[70]

CH_3OH desorption is challenging, since the intermediates are strongly bound to the active site. Overoxidation products are easily formed and desorption leads to unstable bare Cu^I species. All of the above dictate the addition of H_2O for product desorption.[62] According to theoretical calculations, the addition of one H_2O molecule to a hypothetical intermediate $[Cu_2(CH_3OH)]^{2+}$ assists the product desorption by the coordination of H_2O on the Cu sites dislocating CH_3OH, reducing that way the desorption energy.[62, 66b, 66c] In the case of anaerobic DMTM conversion

over Cu-MOR, the addition of H_2O is suggested to relax the system leading to the release of CH_3OH leaving behind a $[CuOH_2Cu]^{2+}$ species which are restored to $[Cu(\mu\text{-}O)Cu]^{2+}$ by H_2 release.[3c] The presence of BAS has been reported to slow down the desorption, attributed to the interaction of CH_3OH with the BAS, suggesting that a high Al content inhibits fast desorption.[53c]

Interestingly Cu-exchanged materials subjected to multiple reaction cycles have exhibited to have a stable performance[3e, 3f, 53i, 60] or even increasing their yield.[3c, 3i, 53h, 71] as well as the selectivity. These results suggest that thermal treatment of rehydrated samples favors the formation of active sites capable for CH_4 activation and that hydration is expected to assist, cycle after cycle, the dispersion of inert Cu ions in the framework leading them into active configurations.[3i, 53i, 71-72] Bozbag *et al.* discussing the yield increment over multiple cycles suggested that subsequent activation of a hydrated sample after a reaction cycle assists the reorganization of Cu species and their electronic and geometrical environment.[71] These evidences corroborate the stability as well as reusability of Cu-exchanged zeolites for the DMTM conversion.

1.3.4. Steady State DMTM Conversion

A step beyond the stepwise DMTM conversion over Cu-exchanged zeolites is the continuous process where formation of active site, CH_4 activation and CH_3OH desorption take place at the same time.[70] Narsimhan *et al.* demonstrated the catalytic steady state operation of the process over numerous structures (MFI, BEA, MOR, FER, FAU and CHA).[54e] After the completion of a DMTM cycle, the materials are subjected to a feed containing P_{CH4} = 98.1 kPa, P_{H2O} = 3.2 kPa, P_{O2} = 0.0025 kPa exhibiting a catalytic reaction at WHSV of 2,400 mL/(h·g_{cat}) where CH_4 is converted to CH_3OH.[54e] Therein, Cu-Na-SSZ-13 (Cu/Al = 0.50) exhibits the highest specific activity of 3.12 $\mu mol_{CH3OH}/(h \cdot g_{cat})$ at 210 °C and a E_{app} of 100 ± 2.1 kJ/mol; tuning the reaction temperature a STY of $31.6 \cdot 10^{-3}$ $molCH_3OH/(molCu \cdot h)$ at 260 °C was achieved. Ipek *et al.* similarly demonstrated the catalytic low-temperature DMTM conversion with N_2O as the oxidant over Cu-SSZ-13, obtaining a CH_3OH production rate of 55 µmol/(g·h) at 300 °C for WHSV of 19,650 $g_{feed}/(g_{cat} \cdot h)$ with 2.3 % CH_3OH selectivity at 0.75 % CH_4 conversion. [55a] Among different frameworks, also their Cu-SSZ-13 showed the higher

production rates.[55a] Despite the fact that catalytic DMTM process is in principle more appealing than the stepwise one because of the absence of temperature swings and constant gas feed, the very low CH_4 conversion reached so far makes it hardly applicable for industrial implementations.[70, 73]

2. Advanced X-ray absorption spectroscopy analysis to characterize Cu-zeolites in the DMTM process

Due to specific fingerprints from Cu and functional groups, spectroscopic techniques such as e.g. XAS, Raman, and Fourier-Transform Infrared (FTIR) spectroscopy [12a, 55c, 74] have proven to be extremely useful in investigating the active sites in Cu-zeolites. When these techniques are used *in situ* and *operando,* they also provide information about spectroscopic changes during the reaction, which can be crucial to understand the reaction mechanism. A peculiarity of XAS is its element-selectivity, and for hard X-ray XAS, its ability to probe the bulk of the material and not only the surface. Since XAS also can also be used under realistic pressure and temperature conditions, it emerges as an incredibly versatile and informative technique. In this section, we discuss different applications of XAS to illustrate how this technique can be used to understand more about the nature of the Cu-sites in various zeolites for the direct conversion of CH_4 to CH_3OH.

2.1. Cu-speciation

As mentioned above, XAS is both an element specific and bulk probing technique, which makes it a highly suitable to investigate Cu-zeolites. However, it also provide an average view on all the absorber-containing species/sites in the sample portion illuminated by X-rays, thus leading to complications with the analysis of the data. Especially in the extended X-ray absorption fine structure (EXAFS), it can be difficult to separate between the contributions of different species. Conversely, the higher effective signal and the presence of well-defined fingerprint peaks in the Cu K-edge X-ray absorption near edge structure (XANES) region, can be advantageous to tackle this inherent limitation of the technique. This section will highlight some recent examples that combine XANES measurements with analysis techniques such as linear combination fitting, principal component analysis and multivariate curve resolution coupled with alternating least squares algorithm, with the aim to determine the structure of the Cu-sites within the zeolite framework.

It is important to stress that XAS is an element selective but average technique. It implies that, in the case of Cu K-edge XAS experiments relevant in this work, the signal exclusively derives

from the Cu-species in the system, but it is averaged over all the Cu-species present, weighted for their relative abundance. The XAS spectrum $\mu(E)$ in a system containing *i* different Cu-species can be thus expressed as the linear combination of the individual spectra $\mu_i(E)$ for each pure species, weighted for their respective fractions w_i: $\mu(E) = \Sigma_i w_i \mu_i(E)$. Once a series of appropriate reference XANES spectra $\mu_i(E)$ is obtained, it is possible to isolate the different contributions by the so-called XANES linear combination fit (LCF) analysis, by evaluating the w_i values providing the best-fit to the experimental spectrum $\mu(E)$.[23b, 53b, 75]

When considering Cu-speciation in dehydrated Cu-zeolites, different Cu^{I} and/or Cu^{II} species coordinated to zeolite lattice oxygens are expected to simultaneously occur, depending on the specific compositional parameters and pre-treatment conditions. Coordination geometry and local environment for such framework-coordinated Cu moieties are quite peculiar and often difficult to reproduce in synthetic model compounds, hence complicating LCF analysis.

If a large enough dataset is available (e.g. from in situ/operando experiments, where the XAS signal is monitored as a function of temperature/time) these difficulties can be overcome by applying a factorial procedure referred to as Multivariate Curve Resolution (MCR), in combination with Principal Component Analysis (PCA). Once the number of Principal Components (PCs) required to explain the variance of the dataset is determined by PCA by means of various statistical indicators, the MCR method enables the decomposition of the original spectral dataset into chemically/physically meaning 'pure' spectra and their concentration profiles along the experiment.[76] To this purpose, the MCR-Alternating Least Squares (MCR-ALS) algorithm is commonly used, where concentration profiles and pure spectra are iteratively optimized in an alternating least squares routine under constraints.[77]

In synergy with the continuous instrumental progresses at synchrotron sources, these statistical/chemometric methods are imposing as essential tools in the interpretation of large XAS datasets.[78] However, an important point to be taken into account during spectroscopic experiments with X-rays is the possibility of radiation-induced alteration of the sample and therefore of the pathways of chemical reactions studied in situ. This problem is particularly relevant for modern beamlines based on insertion devices (wigglers and undulators). Therefore, for each particular sample it is advisable to determine the maximum exposure time that does not lead to significant beam damage. It can be done, for example, by monitoring the

evolution of the spectra collected sequentially under static conditions, or comparing the data collected with and without beam attenuators. If the maximum exposure time it is too low to obtain data of acceptable quality, measures aimed to minimize the radiation-induced effects must be taken, such as increasing the spot size on the sample defocusing the beam or combining measurements in different regions of the sample. Another commonly adopted strategy is cooling down the sample to cryogenic temperatures, but this approach is hardly applicable to in situ catalytic studies.

In the following, we will discuss recent studies highlighting the potential of the advanced data analysis approaches presented above to access a quantitative understanding of Cu-speciation in zeolites, as well as correlation between speciation and DMTM activity.

The Cu-speciation in the DMTM process has been investigated for several years, and already in 2015, Alayon *et al.* studied Cu-MOR (Si/Al = 11 and Cu/Al = 0.38) using XAS during high temperature activation in He and O_2. It was shown that in the case of O_2 activation, two Cu neighbors with 2.29 Å distance are bridged by one oxygen, which is not the case for He activation.[53a] To complement the EXAFS results, the authors employed DFT calculations showing that for MOR, the mono(μ-oxo)dicopper is the more energetically favored compared to bis(μ-oxo)dicopper.[53a] This is in line with evidences from Raman.[3a, 79] Their results were confirmed by Brezicki *et al.*, reporting a first shell coordination number of 2.9 ± 0.2 consistent with $[Cu(\mu\text{-}O)Cu]^{2+}$ or $[Cu(\textit{trans}\text{-}\mu\text{-}1,2\text{-}O_2)Cu]^{2+}$.[25b]

Grundner *et al.* suggested trinuclear Cu-oxo clusters $[Cu_3(\mu\text{-}O)_3]^{2+}$ in the side pocket of MOR, as the active site for DMTM conversion. The normalized product yield for the samples in that study (accounting for CO, CH_3OH, CO_2 and $(CH_3)_2O$) was 0.33 mol(C1)/mol(Cu), suggesting a uniform dominant active site configuration involving three Cu atoms.[3e] EXAFS fitting based on a DFT derived model indicated that such structure would be compatible with experimental data.[3e] The same structure was also suggested to possibly exist in Cu-ZSM-5.[54d]

Both for Cu-SSZ-13 and MOR, the composition (Si/Al and Cu/Al ratios) has been reported to affect the speciation, since Al distribution can alter the concentration and nature of the different Cu docking sites. Sushkevich *et al.* studied MOR samples by varying the Si/Al ratio from 6.5 to 46, suggesting that it controls the speciation of Cu.[53c] It was demonstrated, that monomeric Cu species are favored at low Al contents, while upon increasing the Al amount

oligomeric species become more abundant. In addition, monomeric Cu species and Cu species with higher nuclearity (binuclear and trinuclear) have been reported to possess different redox activity, as observed from CH_4-TPR coupled with XAS studies, which correlates with their activity towards the DMTM conversion.[25b, 53c, 80] The speciation in MOR-zeolites will be discussed in more detail below.

The complex speciation in Cu-SSZ-13, deviating from the single-site model, was initially challenged with H_2-TPR experiments by Kwak *et al.*,[23f] where depending on Cu loading the authors identified two different reduction peaks attributed to redox active and redox resistant Cu^{II} species.[23f] In 2016 Paolucci *et al.* combining DFT calculations with experimental work rationalized the composition derived speciation; reporting a compositional phase diagram (Figure 2.1) where Cu speciation is illustrated as a function of Cu/Al and Si/Al ratios for O_2-activated Cu-SSZ-13.[23a] The identification of 1Al 8MR $[CuOH]^+$ and 2Al 6MR Cu^{II} species in Cu-SSZ-13 as the redox-active and redox-resistant species respectively, is a major contribution to the overall understanding of the Cu-SSZ-13 speciation.[23a, 23f, 23o, 27b] In detail, Figure 2.1 illustrates how the Cu and Al content dictates the speciation. Low Si/Al and Cu/Al ratios lead to solely redox inert 2Al Z_2Cu^{II} in the 6MR species. Increasing both ratios, redox active species (i.e. 1Al 8MR $[CuOH]^+$) form progressively, and at high Si/Al (45) and Cu/Al (0.5) these species are proposed to account for 100 % of Cu.[23a]

Martini *et al.* took a step forward into understanding this complex issue by employing *in situ* XAS coupled MCR-ALS method, providing insights into the effect of composition, temperature and gas atmosphere (O_2 and He flow) on the dynamic nature of Cu ions in the framework.[27a, 81] The work was focused on a large compositional series of Cu-CHA zeolites followed by conventional Cu K-edge XAS during He-activation.[27a] From PCA and MCR-ALS analysis of the global composition- and temperature-dependent dataset, five principal Cu-species were highlighted to form along the process. These species were mobile, fully-hydrated Cu^{II} ions that form four-coordinated Cu^{II} intermediates upon heating, before converting into framework-coordinated $[CuOH]^+$ and bare Cu^{II} species, at 1Al and 2Al sites, respectively. It was proposed that the $[CuOH]^+$ species self-reduce after 200 °C while at 400 °C Cu exists as species in 1Al sites in their oxidized $[CuOH]^+$ or reduced ZCu^{I} forms as well as reduction resistant Cu^{II} species in 2Al 6MR.[27a] In addition, intermediate Si/Al ratios were discovered to contribute to the

reducibility of Cu-CHA, whereas at higher Si/Al ratios the 8MR $[Cu^{2+}OH]^{+}$ species were much more resistant to reduction.

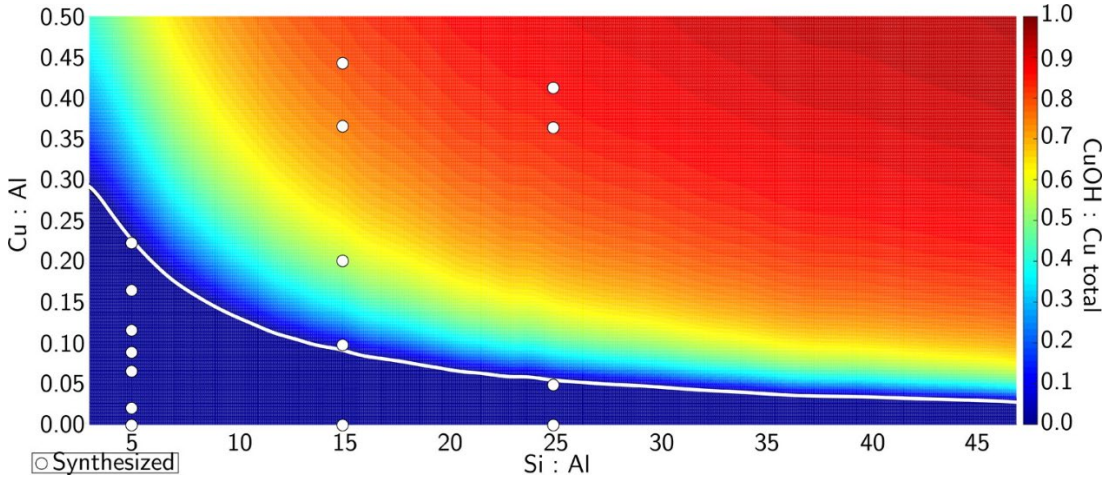

Figure 2.1. Predicted Cu site compositional phase diagram versus Si/Al and Cu/Al ratios. The color scale indicates the predicted fraction of CuOH. The line on the plot demarcates the transition from $[Z_2Cu^{2+}]$-only region to mixed $[Z_2Cu^{2+}]$/[ZCuOH] region. Figure adapted from Paolucci et al.[23a]

Later, Martini et al. continued their work of coupling MCR-ALS analysis with *in situ* XAS for the DMTM conversion over Cu-CHA.[81] They elaborate on how the use of MCR-ALS analysis helps getting one step closer to unravel the Cu-speciation in Cu-zeolites. The authors collected high energy resolution fluorescence-detected (HERFD) XANES on a Cu-CHA with Cu/Al = 0.5 and Si/Al =15 during activation in both O_2 and He, to obtain better energy resolution of the spectra and therefore higher precision in determining the independent components. For a satisfactory reconstruction of the dataset, six components were necessary, in contrast to five described in the previous study of He activation. The successful identification of an additional component shows the importance of taking all possible measures to obtain the best signal to noise ratio and energy resolution when collecting XAS spectra, as well as to obtain large enough datasets suitable for statistical analysis. In this respect, the use of HERFD XANES at an undulator beamline could represent an important advantage. The principal components were linked in this case to hydrated Cu^{II} (PC1), ZCu^{I} (PC2), Z_2Cu^{II} (PC3), $ZCu^{II}OH$ (PC5) and under-coordinated Cu^{II} dehydration intermediate (PC6). The extra component not found previously is an O_2-derived Cu^{II} species (PC4). The authors suggest that the extra component observed is crucial for the activation of CH_4. This is based on this component being the dominant Cu-species after O_2-activation (70 % of the Cu at the end of the protocol) and almost undetectable after He-activation. The component PC5 ($ZCu^{II}(OH)$) is present in a large abundance before it undergoes

self-reduction to ZCu^{I}. The XANES spectra and the fraction of the different components are presented in Figure 2.2.

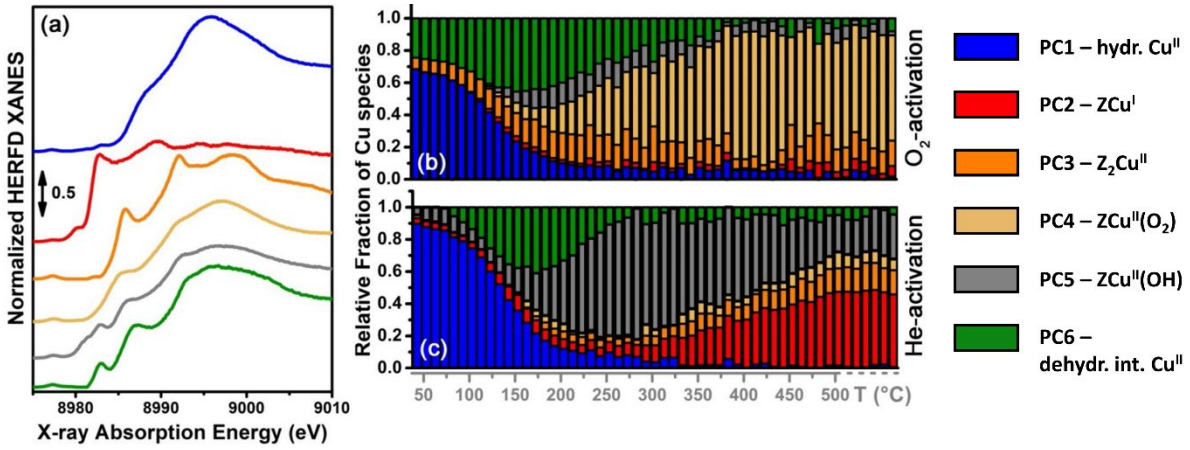

Figure 2.2. (a) Pure XANES spectra obtained from combining MCR-ALS analysis of *in situ* HERFD XANES data collected during O_2- and He-activation of Cu-CHA (Cu/Al = 0.5, Si/Al = 15). The concentration profiles during (b) O_2-activation and (c) He-activation obtained from the pure spectra reported in (a) are given as a function of the correspondent data collection temperature. The color code given for the principal components (PC1-PC6) is the same throughout the figures. Adapted from Martini et al. [81]

PC5 is the same species that is suggested as a precursor for the active sites in Cu-CHA.[3i] This will be discussed further in section 2.2. PC4 and PC5 have very similar spectral features, and it was hardly possible to separate these two components with MCR analysis of the conventional transmission-mode XANES spectra as reported previously by Martini et al.[27a] Collecting the XANES data in HERFD mode proved therefore to be crucial in order to disentangle these two structural components. The difference was observed by a slightly sharper and more intense main maximum (so-called white line) as well as a 1 eV red-shift of the energy position of the rising edge peak compared to PC5. The authors do assign the PC4 component to a three-fold coordinated species due to the similarities of the XANES spectra compared to $ZCu^{II}(OH)$, however, they have only suggestions as to what species the PC4 component is. Several candidates fit the criteria, and among them: monomeric end-on $Z[Cu^{II}(O_2)^{-}]$ superoxo species or dimeric trans-(μ-1,2-peroxo) and mono(μ-oxo) Cu^{II} moieties. This is in good agreement with results obtained by Pappas et al.,[3i] which will be discussed in more detail in section 2.2.

MCR-ALS analysis coupled with XANES was also used by Pappas et al.,[53g] who did a thorough study on the speciation in MOR zeolites. With the use of two H-MOR materials (Si/Al = 7 and Si/Al = 11), they prepared six samples containing a low, medium and a high loading of Cu from each parent. One material (Cu-MOR with Cu/Al = 0.18 and Si/Al = 7) was outperforming the

others, with a productivity of 0.47 molCH_3OH/molCu, giving a yield as high as 170 µmol/g at 1 bar methane loading. The high productivity of this material indicates an almost perfect two-to-one ratio of Cu atoms per CH_3OH, indicating that this material has a performance close to maximum, assuming that the active sites consists of dicopper species. To understand more about the outlying high performance of the medium-loaded material (Cu/Al = 0.18, Si/Al = 7), the authors attempted to rationalize the trends observed by *operando* XAS at the Cu K-edge on four of the samples. XANES and EXAFS spectra collected for the four samples during different treatments (O_2-activation, He-flushing and reaction with CH_4 and steam) exhibited similar features, suggesting similar geometry and coordination environment for the Cu ions. Nonetheless, differences were observed in the intensities of the features. During O_2-activation at 500 °C a higher white line intensity is observed for materials with lower Cu/Al and Si/Al ratio, leading to the trend: Cu-MOR (Cu/Al = 0.18, Si/Al = 7) > Cu-MOR (Cu/Al = 0.24, Si/Al = 7) > Cu-MOR (Cu/Al = 0.28, Si/Al = 11) > Cu-MOR (Cu/Al = 0.36, Si/Al = 11). The same trend is observed in the first and second shell peak of the FT-EXAFS spectra. The first shell was previously assigned to the scattering coming from framework (O_{fw}) and extra-framework (O_{ef}) oxygen atoms.[23o], [3e, 53a] The higher intensity of the first shell and the white line is usually identified with the Cu ion having a higher coordination number (CN), in addition to a more uniform distribution of the interatomic distances.

The second shell intensity, on the other hand, was found to directly correlate with the normalized productivity of the materials. The reason for this is that the second shell peak is associated with Cu-T_{fw} and Cu-Cu scattering (T_{fw} being Si or Al atom of the zeolitic framework). Cu-T_{fw} scattering should be equally present in monomeric and multimeric Cu^{II} moieities since each Cu atom attached to the framework in any case sees only one T_{fw} atom in its nearest vicinity, regardless of the nuclearity of Cu site. The Cu-T_{fw} contribution should therefore be the same for all MOR materials. So, if a higher intensity is observed for the second shell peak, it is due to Cu – Cu scattering, which is a direct indication of multimeric Cu_xO_y species in the materials. Due to this, authors suggest that a higher intensity of the second shell peak can be directly correlated with a higher fraction of active Cu.

As also mentioned previously, since XANES is an averaging technique, and some of the different framework-coordinated Cu species exhibit similar spectral features, collection of

XANES spectra with high energy resolution is beneficial for successful discrimination between such Cu-species. Therefore Pappas et al.[53g] collected HERFD XANES spectra of the two most outlying Cu-MOR materials (with Cu/Al = 0.18 and Si/Al = 7 and Cu/Al = 0.36 and Si/Al = 11) in order to increase the contrasts between the different contributions from active and inactive species in the XANES region. With MCR-ALS analysis, they separated the different contributions, quantifying the speciation after activation in both O_2 and He flow (500 °C). It was found that the Cu speciation during He- and O_2-activation can be described by linear combination of five Cu-species. Among these species, two were found to be framework-coordinated Cu^{II} species (fw-Cu^{II} species), where one was prone to self-reduce in He to Cu^{I} already at 250 °C (PC3), while the other component is stable all the way to 400 °C (PC5). Using the obtained components, the spectra of all samples collected after O_2 activation were analysed to determine and correlate the fraction of active Cu species formed to the productivity per Cu. The authors linked PC5 to multimeric Cu-oxo cores, due to the enhanced stability predicted for these species compared to monomeric Cu^{II} species such as [Z-Cu^{II}OH].[82] Further, they observed that the PC5 component was much more abundant in the highly performing Cu-MOR (Cu/Al = 0.18, Si/Al = 7) after O_2-activation, as can be seen Figure 2.3 (b). In the HERFD XANES spectra, the PC5 component gives rise to more intense and narrow rising-edge and white-line peaks. Since the PC5 component is present in some of the studied materials also in inert environment it does not exclude the alternative of having an anaerobic reaction process as suggested previously by Sushkevich, van Bokhoven and coworkers.[3c] However, under the standard conditions, replacing the oxidizing atmosphere with inert gas does lead to a huge reduction in productivity, suggesting that a prolonged exposure to O_2 is necessary for transforming inactive Cu (or precursors) into active species. The geometric insights obtained from operando EXAFS as well as the pure HERFD XANES signature of PC5 both indicate that the active sites are dimeric Cu-species, such as a mono-(μ-oxo) dicopper(II) core or a trans-(μ-1,2-peroxo) dicopper(II) core. These findings corroborate the results obtained previously by Alayon *et al.*, who utilized DFT and proposed [Cu^{I}O-CH_3Cu^{II}] and [Cu^{I}OHCu^{II}] as possible intermediates for the CH_4 activation over Cu-MOR. This pathway requires two active sites per CH_3OH atom produced.[53b] The interaction of O_{ef} (extra-framework oxygen atoms), bound on Cu with CH_4 was also shown using *in situ* ambient-

pressure X-ray photoelectron spectroscopy, suggesting the CH_4 activation occurs on the activated O_{ef} rather than the O_{fw} (framework oxygen atoms).[83]

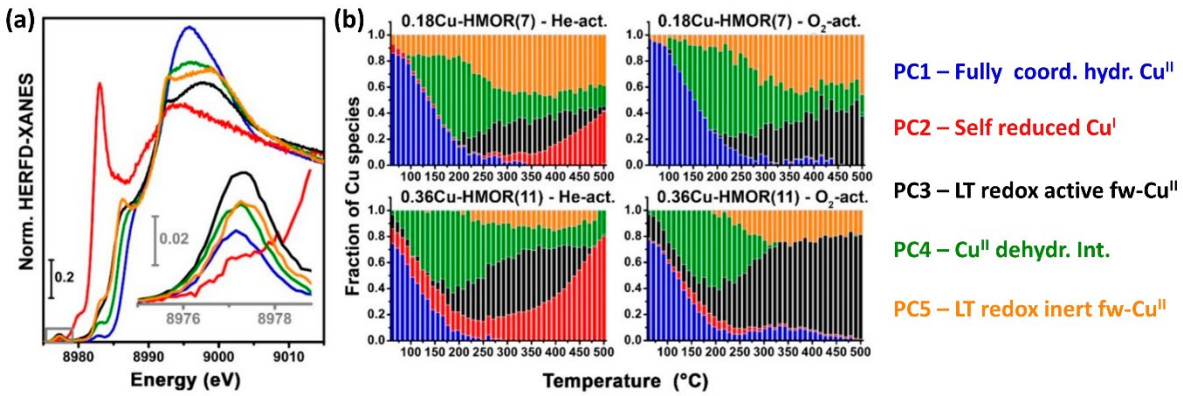

Figure 2.3. (a) Pure HERFD XANES components obtained from MCR-ALS analysis of data collected from O_2- and He-activation of Cu-MOR (Cu/Al = 0.18, Si/Al = 7) and Cu-MOR (Cu/Al = 0.36, Si/Al = 11). (b) Temperature-dependent concentration profiles of species PC1-PC5 during He-activation and O_2-activation obtained from the pure spectra reported in (a). The color code for the principal components (PC1-PC5) is the same throughout the figure. Adapted from Pappas et al. [53g]

In a later publication, Borfecchia et al.[53f] reported a detailed comparison of two different Cu-zeolite materials namely CHA and MOR, monitored at consistent conditions throughout all the steps of the DMTM conversion. A low (LL) and a high (HL) Cu-loaded CHA and MOR (Si/Al = 12 and 11, respectively), denominated LL Cu-CHA, HL Cu-CHA, LL Cu-MOR and HL Cu-MOR, were investigated. The Cu-MOR materials outperformed the Cu-CHA. This is linked with the possibility that a significant fraction of the Cu-species in Cu-CHA are present as inactive 2Al Z_2Cu^{II} sites hosted in the 6MR of the CHA framework as discussed above and illustrated in Figure 2.2. XANES and EXAFS spectra of Cu-zeolites after O_2-activation, He-flushing, CH_4-loading and CH_3OH-extraction were collected and compared meticulously with an attempt to find changes that could be assigned to specific structural changes in the active sites. In general, Borfecchia et al. observed a similar shape and behavior of all the collected spectra, indicating that the Cu-sites are likely to have similar structural environment. During O_2-activation, however, differences in the shape and intensity of the white line were observed, with the LL Cu-CHA having the highest intensity, in agreement with this material having a higher fraction of Z_2Cu^{II} species in the 6r 2Al sites. This is further supported by a higher coordination number in both the first and second shell of the FT-EXAFS as well as a longer Cu-T_{fw} distance of the LL Cu-CHA compared to the HL Cu-CHA. Cooling to 200 °C with subsequent flushing with He leads to an increase in white line intensity as well as the first shell peak of all materials. This feature

is correlated to thermally induced modifications to the Cu-coordination, which the authors suggest to stem from the Cu-coordination changing from Cu-superoxo end-on to a side-on configuration.[53f] This corroborates evidence previously obtained from Raman spectroscopy.[3i] Based on spectroscopic development observed during the CH_4 loading, the authors conclude that the active Cu-sites have to be part of the Cu^{I} component that is formed during CH_4-loading. When investigating the CH_3OH extraction step, they observe an intense white line and a flat rising-edge region in the XANES spectra, which they attribute to the formation of hydrated Cu^{II} species. These XANES results suggests that a redox reaction occurs at the metal centers when steam is passed through the reactor, which also indicates that it is possible to make an anaerobic process as already discussed above.[53c] A summary of proposed Cu-species at each step of the conversion is thus illustrated in Scheme 2.1.

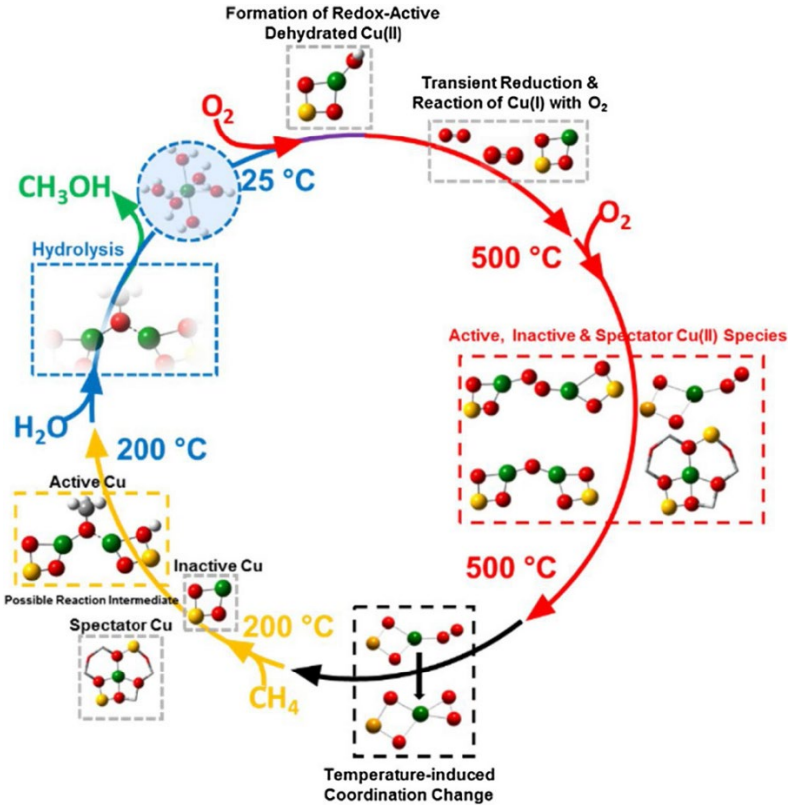

Scheme 2.1. Representation of proposed Cu-speciation for the different stages of the DMTM process. The structures are based on literature and the XAS data presented by Borfecchia et al.[53f]

2.2. Reducibility – activity relationships

It is clear from the literature examined so far that the redox properties of the material are important when comparing Cu-zeolites for the direct conversion of CH_4 to CH_3OH. As we will exemplify in more detail below, XAS is a highly sensitive technique to obtain information about the reducibility of the material and to correlate it to the productivity.

In 2017, Pappas et al.,[3i] based on an investigation of Cu-CHA materials, optimized the process conditions and material composition that provided the highest yields reported to date for Cu-CHA. After observing that the change of process parameters had a huge impact on the CH_3OH yield, they followed up with an investigation of the activation conditions with XAS. *In situ* and *operando* XAS was employed to investigate the changes after each step of the reaction. Pappas et al. analyzed the XANES features observed by comparing with previous Cu K-edge studies on Cu-zeolites, also aided by the vast literature available for Cu-containing metallo-enzymes.[12a] The O_2-activated material appeared to be in a pure Cu^{II} state, as determined also by several other groups.[23a, 23l, 23o] During CH_4 loading, the characteristic Cu^{I} peak at ~8983 eV starts appearing, together with a small intensity decrease of the dipole-forbidden 1s → 3d transition in Cu^{II} ions. This indicates the partial reduction of Cu^{II} to Cu^{I} (~27 %). The authors find that 13 % of the Cu^{I} species are reoxidized to Cu^{II} during the CH_3OH-extraction on accord with the productivity per Cu of 0.1 molCH_3OH/molCu. The *operando* XANES and EXAFS spectra as well as the fractions of different types of Cu-species, estimated by XANES LCA analysis, are presented in Figure 2.4.

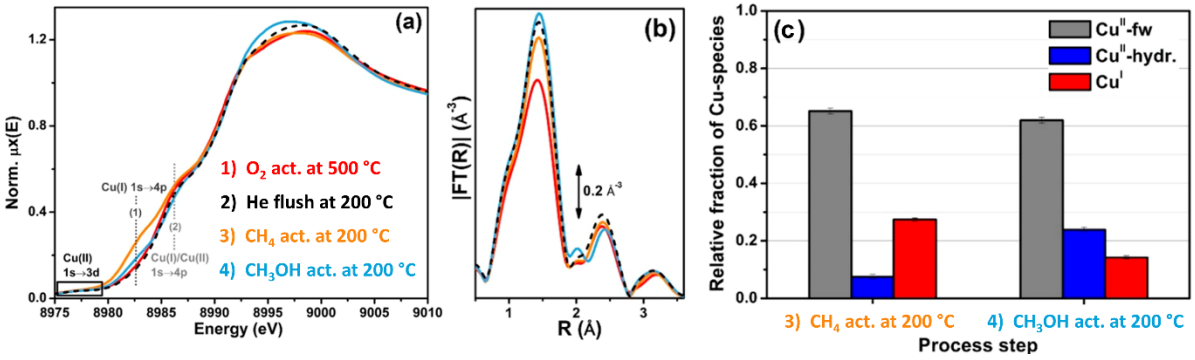

Figure 2.4. *Operando* XANES and EXAFS collected after each step of the DMTM conversion on Cu-CHA (Cu/Al = 0.5, Si/Al = 12). Cu K-edge XANES spectra are shown in (a), and the corresponding FT-EXAFS spectra are shown in (b). Panel (c) shows the relative fraction of different Cu-species determined by LCF of the XANES data in (a) after CH_4 loading (left) and CH_3OH extraction (right). Adapted from Pappas et al. [3i]

After performing LCF analysis on the *in situ* XANES data of different activation conditions (O_2 and He), the authors find a linear correlation between three samples with different Si/Al ratio (Cu/Al = 0.5, Si/Al = 5, 15 and 29), when they compare the productivity ($molCH_3OH/molCu$) to the relative fraction of Cu^I at 500 °C in He (Figure 2.5).

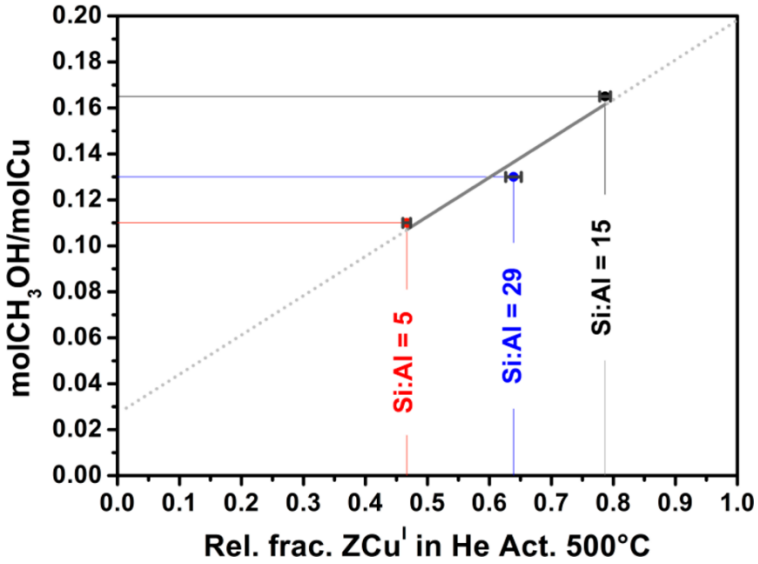

Figure 2.5. Correlation of the normalized productivity of three different CHA materials to the relative fraction of Cu^I obtained from LCF of XANES collected during He activation at 500 °C. Adapted from Pappas et al.[3i]

With the use of previously reported MCR-ALS data (the same principal components as reported by Martini et al. in the work discussed above[27a]), the authors suggest the presence of 2Al ZCu^{II} species and 1Al[$ZCu^{II}OH$] after activation. The material with the lowest Si/Al ratio has the highest fraction of the inactive 2Al ZCu^{II} species, rationalizing the lower DMTM reactivity, and falling perfectly in line with the diagram from Paolucci et al.[23a] (Figure 2.1). 1Al[$ZCu^{II}OH$] species are suggested to be precursors for the active sites because of their ability to self-reduce. The self-reduction reaches an optimum at intermediate Si/Al ratios. The 1Al[$ZCu^{II}OH$] species thus evolve into mono- and multimeric Cu_xO_y-species during the O_2-activation, among which the active species for CH_4 activation are present. The latter are expected to be similar to those reported for Cu-MOR and discussed in the section 2.1.

Later, the reducibility in various Cu-zeolites (MOR, MFI, BEA and FAU) was also investigated in the context of the DMTM reaction. Sushkevich et al.[80] report that the transition from Cu^{II} to Cu^I, when heating in He, occurs gradually over the materials. All the materials showed similar behavior, with the exception of one extra peak appearing at elevated temperatures for Cu-FAU. At T= 577 °C, a peak appeared at 8989 eV, indicating that Cu-FAU has another Cu^I species

with different electronic and local properties. This indication is later corroborated with the use of IR-spectroscopy of adsorbed NO.[68] With the use of linear combination fitting of the Cu K-edge XANES spectra (LCF-XANES), Sushkevich et al. took it a step further, and were able to access the fraction of Cu^{I} species obtained when heating the O_2-activated spectra in He.[80] Interestingly, after heating to 677 °C, there were still a fraction of Cu^{II} left in the materials. Depending on the zeolite material, the self-reduction of Cu in the materials reached around 60 – 80 % of Cu^{I}, when heated in He. Another interesting finding by Sushkevich et al. was the modification of the redox properties of Cu-MOR zeolites as a function of Si/Al ratios. A higher Si/Al ratio leads to an increase in the temperature required for Cu reduction. The temperature varies from 333 °C for the material with Si/Al ratio of 6, and up to 433 °C when the Si/Al ratio is 46. Conversely, no differences were observed when the Cu loading was varied for one of the MOR at fixed Si/Al = 6. The LCF analysis of the three cases is presented in Figure 2.6. A higher Cu reduction temperature is likely related with a longer distance between the Cu ions and second-nearest Al center, which might be required for efficient self-reduction.[27a] That would explain the low reduction temperature for MOR (Si/Al = 6), where the Al centers are always in a close proximity, likely leading to more dicopper species. Based on the results, combined also with FTIR spectroscopy, the authors suggest that self-reduction is favored in materials that form Cu-oxo oligomers, such as MOR and MFI zeolites.

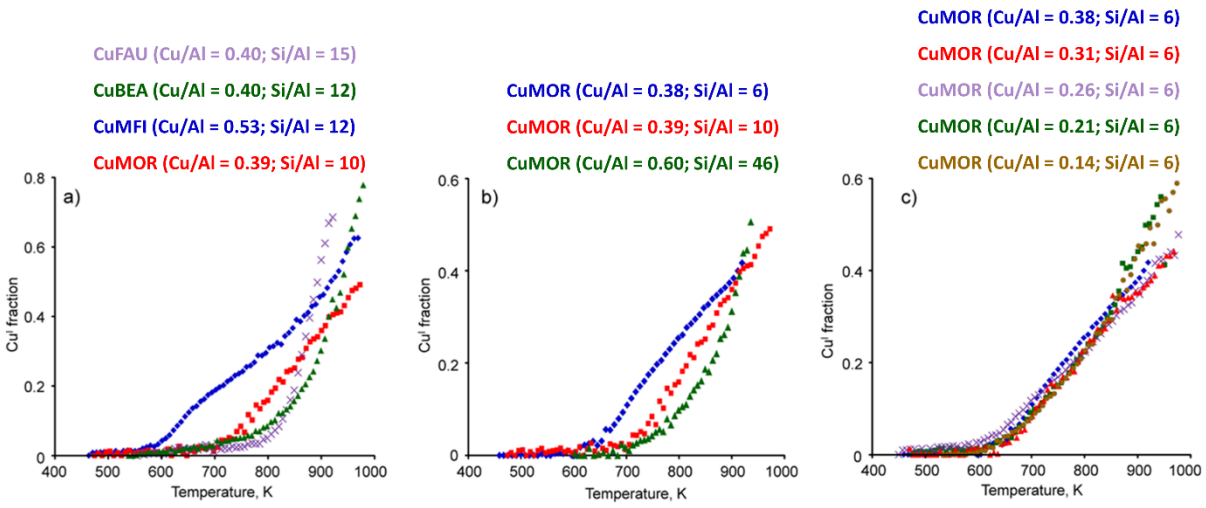

Figure 2.6. LCF analysis of the XANES spectra collected during the reduction in He. The three plots represents (a) different zeolite topology, (b) Cu-MOR samples with different Si/Al ratio and (c) different Cu loading. Adapted from Sushkevich et al. [80]

Sushkevich et al. continued to analyze these materials (MOR, MFI, BEA and FAU) by combining XANES with CH_4-TPR to obtain a deeper understanding about the redox properties of the Cu-sites in the materials.[68] They acquired XANES spectra during heating from 100 to 473 °C of the four materials. LCF analysis of the XANES data shows that Cu-MFI and Cu-MOR have a faster reduction time, while the reduction of FAU and BEA occurs more gradually from 177 to 477 °C. From comparing the LCF-XANES data to CH_4-TPR, they observe that the temperature corresponding to 50 % conversion of Cu ions in the probed sample to Cu^I increases as follows for both characterization methods: Cu-MFI (Si/Al = 12) < Cu-MOR (Si/Al = 10) < Cu-BEA (Si/Al = 12) < Cu-FAU (Si/Al = 15). Based on the results above, and previous findings, it evidences that the Cu-oxo oligomers found to be present in Cu-MOR(Si/Al = 10) and Cu-MFI (Si/Al = 12) undergo reduction with CH_4 at low temperatures. The Cu sites in Cu-BEA (Si/Al = 12) and Cu-FAU (Si/Al = 15), however, appear to require much higher temperatures for complete reduction. Since the reduction also occurs over a wider temperature range, these materials are likely to have more than one Cu-site. It is in line with the change in temperature that was observed for the series of Cu-MOR with different Si/Al ratios, where higher Si/Al ratio leads to more isolated Cu-species.

The results presented by Sushkevich et al.[68, 80] show that the activity and selectivity of Cu-exchanged zeolites are governed by their redox properties. Under the process conditions for the stepwise conversion of CH_4 to CH_3OH, where CH_4 is loaded at 473 K at 8 bar for 30 min, it becomes apparent that materials with a higher reduction temperature has lower CH_4 conversion. Concomitantly, high productivity has been obtained for Cu-MOR materials working at a temperature at ~200 °C for CH_4 activation, whereas Cu-FAU has been almost inactive at the same conditions.[68] By increasing the CH_4 activation temperature to 360 °C to maximize the reduction of Cu-FAU, Sushkevich et al. observed a five times increase in the productivity of this material compared to 200 °C (25 µmol/g). Moreover, after tuning Cu-loading and CH_4 activation pressure, they obtained for Cu-FAU a very high CH_3OH yield of 360 µmol/g.[68] This is an important advance in the context of process optimization, since the methane loading temperature of 360 °C is close to the temperature at which the material is activated in O_2 (500 °C), which allows to decrease the associated temperature swing.

An important technical point of the linear combination XANES analysis is the choice of the reference compounds. The general rule of thumb would be that the structures of the references for Cu^{I} and Cu^{II} has to be as close as possible to those of the actual samples. Thus, in the studies of Sushkevich et al. [68, 80], spectra collected after treatment of the samples in oxygen at 673 K and in methane at 800 K were used as the standards for Cu^{II} and Cu^{I}, respectively. Conversely, the use of, for example, Cu^{I} and Cu^{II} oxides as references would be inappropriate for the zeolite samples where Cu sites remain isolated throughout the studied process.

Reducibility of Cu species probed through self-reduction in inert atmosphere, or via interaction with CH_4, appears to be influenced by the proximity of Cu species and adjacent BAS, both depending on the Cu/Al, Si/Al ratio and Al distribution. Based on the above considerations, it appears that for DMTM conversion an optimum Si/Al ratio is required in order to form redox active sites existing in close proximity, while avoiding bare Cu^{II} in small rings, such as 6MR in CHA.[3h, 28, 72] . Interestingly, the recent reports from Dyballa et al.[84] and Sushkevich et al., [85] present a combination of FTIR and NMR spectroscopy as a tool to investigate the stabilized CH_4 after activation. Intriguingly, the authors suggest that the reaction generates stable methoxy groups attached to BAS, indicating the need for BAS in combination with Cu-sites in the zeolite for a high DMTM performance.

2.3. Towards the understanding of the reaction mechanism for DMTM over Cu-species

Here we will discuss how XAS, alone or combined with other techniques, can be used to determine the nature of the redox mechanism taking place during the DMTM conversion over Cu-zeolites, and thereafter correlating the Cu concentration in the materials to the yield of CH_3OH. Some possibilities are that the mechanism is based upon a Cu^{I}/Cu^{II} couple,[3a, 3i, 28, 53b, 66c, 86] Cu^{II}/Cu^{III} couple[3e, 3g, 53i, 66c] or *via* Cu^{II}-O• radicals.[87] However, from the XAS data presented thus far, a mechanism based on Cu^{I}/Cu^{II} finds most support due to the clear evidence of Cu^{I} from the spectra of the samples after the interaction with methane. In addition, no spectral features indicating the presence of Cu^{III} in the reaction conditions have been unambiguously identified so far.

Van Bokhoven and coworkers have provided a great deal of insight into this topic over the last years. Newton et al.,[88] investigated four different Cu-exchanged zeolites (MOR, MAZ, CHA and MFI) with *in situ* Cu K-edge XANES during activation in O_2 at 450 °C and isothermally by activation in O_2 at 200 °C, followed by high pressure CH_4 loading (from 6 to 15 bar). As was discussed previously, the O_2-activated state at high temperature appear to be pure Cu^{II}. After exposure to CH_4, a transition from Cu^{II} to Cu^{I} is observed. In Figure 2.7a, a calculated ratio of Cu^{I} per CH_3OH is presented, produced by comparing the fraction of Cu^{I} calculated from LCF analysis of the collected XANES spectra of different sets of zeolites to their yield of CH_3OH (μmol/g). Interestingly, the Cu^{I}/CH_3OH ratio seems to lie mostly in the range of 2-3, which suggests a two-electron Cu^{I}/Cu^{II} redox couple that has a high selectivity towards CH_3OH, therefore excluding a mechanism based on a Cu^{II}/Cu^{III} couple.

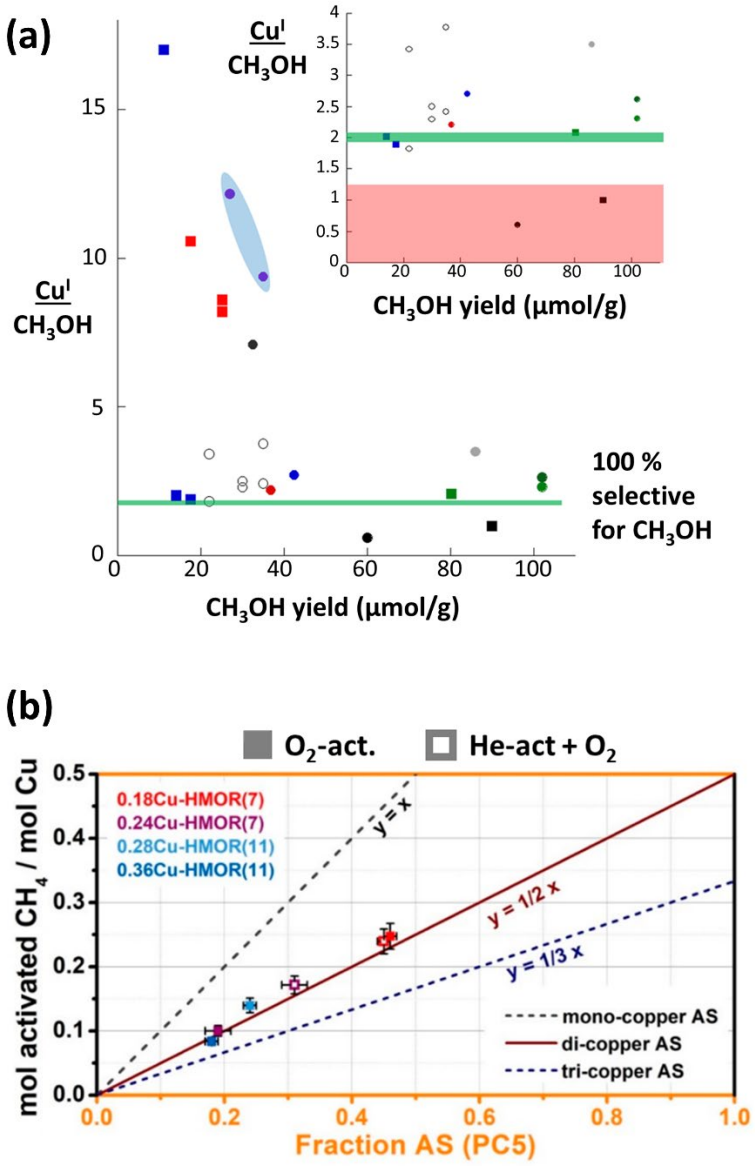

Figure 2.7. Comparison (a) of the Cu^{I}/CH_3OH ratio to the CH_3OH yield of various Cu-zeolites collected at different process conditions. The inset shows an enhancement of the lower region where the concentration of data points is highest. The green line represents an ideal Cu^{I}/Cu^{II} redox scenario. High-temperature activation of Cu-MOR samples of different composition is presented in red, blue, green, dark green and black solid circles. The empty circles are Cu-MOR collected under isothermal conditions (200 °C, 6 – 15 bar). MAZ (light grey), CHA (dark grey) and ZSM-5 (purple with the blue shaped ellipse) collected after high-temperature activation are also presented. In the bottom panel (b), the quantitative correlation between productivity and the fraction of the presumed active site, PC5, is plotted for the data presented by Pappas et al.[53g] The experimentally determined values correlate with a trend line for a dicopper active site. Panel (a) is adapted from Newton et al.[88]Panel (b) is adapted from Pappas et al. [53g]

This result fits well with evidence from the MCR-ALS analysis by Pappas et al., discussed above.[53g] All the evidence collected from PCA and MCR-ALS of the HERFD XANES correlated with the operando XAS data, lead the authors to identify the active species (designated PC5) for the DMTM conversion over Cu-MOR. By comparing the productivity per Cu obtained from activity tests, performed at the same reaction conditions as used under the HERFD XANES

collection, to the fraction of PC5, which they obtained by XANES LCF, an interesting trend was observed. The data points fell into a linear trend matching a dicopper(II) active site, compatible with a redox mechanism corresponding to a Cu^{I}/Cu^{II} couple (Figure 2.7b), in line with the proposal by Newton et al.[88]

Another insightful study was recently reported by Knorpp et al.,[63] who investigated the reaction mechanism over Cu with XAS coupled with TGA. A comparison of a high temperature activation and an isothermal (high CH_4 pressure) route at 200 °C was performed, in order to observe possible variations in the structure and activity of the investigated Cu-MOR zeolite. XANES-LCF analysis of hydrated materials shows that the Cu ions are not fully dehydrated until they are heated at ~350 °C, as also previously observed with FTIR by Pappas et al.[3i] Although a large fraction of Cu centers is already dehydrated at 200 °C, the authors determine that at that temperature there are still 1.6 water molecules per Cu left in the pores, and therefore water-stable active sites that have previously been suggested[53b, 54e, 89] are more likely to form than conventional high temperature dimeric or trimeric structures. It appears that the yield from these site increases with increasing CH_4-pressure, along with the increase in reduction of Cu^{II} to Cu^{I} as observed with XANES. Focusing on the isothermal procedure, the authors investigate pressure-dependent changes in the XANES data and correlate them with the CH_3OH yield. This leads to a quantification of the number of electrons used per CH_3OH formed. The authors observe a ratio of Cu^{I}/CH_3OH close to 2, in agreement with the abovementioned two-electron redox mechanism involving a Cu^{I}/Cu^{II} redox couple.

The reaction mechanism was investigated also for Omega (MAZ) zeolites.[56] MAZ has been shown to have comparable CH_3OH yields to MOR, although the literature on this material for the DMTM conversion is scarce.[53e] *In situ* XANES spectra on MAZ zeolites with varying Cu-concentration (1.5 – 4.7 %) were collected during both activation in O_2 (450 °C) and subsequent reaction with CH_4 (200 °C). The authors show with FTIR that MAZ has very distinct Cu-sites, which are good for stabilizing methoxy species. This behavior leads to MAZ having a very high selectivity towards CH_3OH. In Figure 2.8, two methods for correlating the amount of participating Cu and the amount of electrons involved to the CH_3OH yield over Cu-MAZ are shown. Both methods show a ratio that is close to 2 for the whole set of samples. The Cu^{I}/CH_3OH ratio indicates that the DMTM reaction over the investigated Cu-MAZ zeolites is

based on a two-electron mechanism for a Cu^{I}/Cu^{II} redox couple. The ratio of active Cu indicates that around Cu-atoms are participating in the reaction on average.

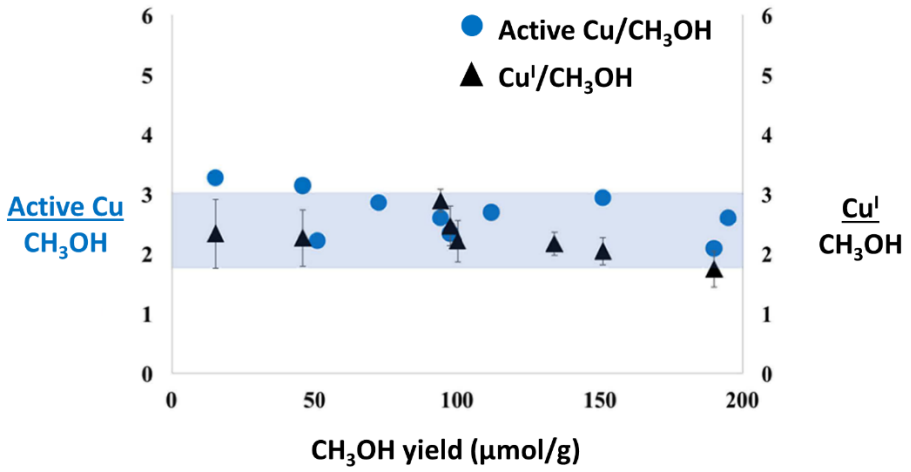

Figure 2.8. Comparison of the Cu^{I}/CH_3OH ratio to the CH_3OH yield (right axis) *vs* the ratio of active Cu/CH_3OH to the CH_3OH yield (left axis) for a set of Cu-MAZ zeolites collected under both 1 and 30 bar of CH_4 loading. Adapted from Knorpp et al.[56]

In an attempt to shed light on the DMTM mechanism based on Cu-MOR materials, Lomachenko et al.[90] recently followed the entire reaction process with *operando* XAS, comprising 8-hour O_2 activation. The authors performed a short (SP) and a long protocol (LP) on two different Cu-MOR zeolites: the high-performance Cu-MOR (Cu/Al = 0.18 and Si/Al = 7) and its much less performing Cu-MOR counterpart (Cu/Al = 0.36 and Si/Al = 11). The difference between LP and SP was in the duration of the activation in pure O_2 at 500 °C (8h for LP, 1.5h for SP) and in the duration of the reaction with pure methane at 200 °C (6h for LP, 2h for SP). During O_2 activation, the materials behave as previously described, with the XAS features pointing to a pure Cu^{II} state. When ramping down to 200 °C and subsequently flushing in He, an intensity increase occurs in the XANES white line as well as the EXAFS first-shell peak. These features have been linked to thermal-induced rearrangement of the structural components, e.g. the change from a Cu^{II}-oxo end-on to a side-on configuration, as also discussed by Pappas et al.[3i] During CH_4 loading and CH_3OH extraction, the authors observe more pronounced changes in the features, such as reduction of Cu^{II} to Cu^{I} and hydration phenomena, which create a path for unraveling the behavior of the Cu-sites during the DMTM conversion. The highly-performing Cu-MOR, with a productivity of 0.47 molCH_3OH/molCu, is likely to possess a very uniform distribution of active sites, where all the Cu ions contribute to the reactivity.

This sample is therefore an optimal material to obtain information on the Cu^{I} species formed during CH_4 activation. With the use of LCF on the sequences of XANES spectra, presented in Figure 2.9, the authors monitored the evolution of abundance of different Cu species with time for the two different materials in the two different protocols. By plotting the CH_3OH productivity per Cu *vs* the fraction of Cu^{I} detected during the CH_4 loading step, the authors observe a linear trend, with a slope close to unity (bottom panel of Figure 2.9). This trend indicates that the production of one CH_3OH molecule succeeds the reduction of one Cu(II) ion to Cu(I) upon exposure to CH_4. It is proposed that the Cu^{I} stems from a mono(μ-oxo) dicopper(II) site, suggesting a mixed-valence configuration of Cu^{II}/Cu^{I} after exposure to CH_4.

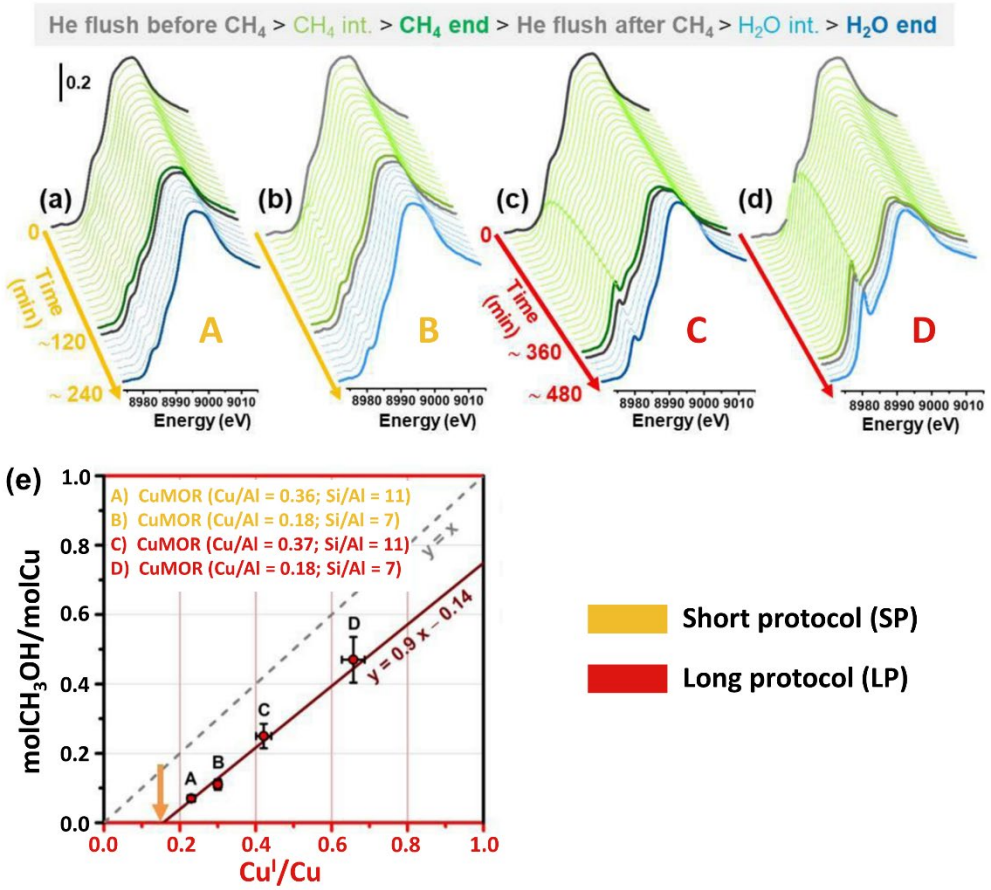

Figure 2.9. The top panel (a-d) shows time-resolved *operando* XANES spectra collected for (a,c) Cu-MOR (Cu/Al = 0.36 and Si/Al = 11) and (b,d) Cu-MOR (Cu/Al = 0.18 and Si/Al = 7) during CH_4 loading and subsequent CH_3OH extraction of the short (a,b) and long protocol (c,d). The plot (e) at the bottom shows a correlation of the normalized productivity to the total fraction of Cu^{I} per Cu after methane loading for the four experiments presented in the top panel. Adapted from Lomachenko et al.[90]

The highest amount of Cu^{I} observed after the CH_4 loading is about 66 %. Having a fraction of Cu^{I} > 50 % total Cu (i.e. one reduced Cu per dicopper active site) could be connected with unselective CH_4 conversion to byproducts different from CH_3OH. Indeed, the trend line has an offset with a negative intercept of – 0.14 molCH_3OH/molCu, which the authors suggest comes from CO_x species formed during CH_3OH extraction that lowers the selectivity, as well as direct oxidation of CH_4 to CO_x during CH_4-loading. That might explain the seeming discrepancies with other studies, where lower-performance materials are studied. Indeed, due to this important offset, at low Cu^{I} contents the observed molCu^{I}/molCH_3OH ratio is indeed between 2 and 3. It is only when materials and process conditions resulting into very high performance are included in the analysis that the linear trend with the slope close to 1 becomes appreciable.

3. Summary and outlook

This review critically summarizes the most recent reports highlighting the potential of XAS, together with advanced data collection and analysis approaches, in understanding more about the reducibility, speciation and reaction mechanism involving the Cu-sites in the direct CH_4 to CH_3OH conversion over Cu-zeolites. We have seen that, since XAS is a bulk averaging technique, it can be challenging to separate the contributions coming from the different Cu-species. The use of PCA and MCR-ALS, especially in combination with high-resolution HERFD XANES, is truly opening the door to unravel the complex nature of Cu-zeolites as well as other metal systems. It is also clear that the activity of Cu-zeolites is strongly correlated to the reducibility of Cu^{II} to Cu^{I}. Presented examples show also how useful it is to combine XAS with other techniques, such as TPR (reductants or oxidants), XRD or FTIR. The determination of the reaction mechanism occurring over the Cu-sites in the DMTM conversion is still an ongoing debate in the field. XAS data obtained by different groups indicate the reaction occurs over a Cu^{I}/Cu^{II} redox couple, and that the active site is most probably a pair of neighbouring Cu atoms. Conversely, the nature of intermediate species and the electron transfer occurring during the process are still the object of vivid debate. With this respect, the synergy between theory and advanced spectroscopic approaches, including XAS-based techniques, is expected

to play a key role in further advancing the molecular-scale understanding of the reaction mechanism.

As pointed out by van Bokhoven and coworkers,[69] to approach the commercialization of the DMTM process it will be important to increase the productivity and reduce the reaction time. Basing on what we already know about the stepwise reaction mechanism, it is possible to suggest that an isothermal approach would be the first step in reducing the reaction time. Ravi et al. indicate that the search for and lack of understanding of the active site should not stand in the way of finding the most optimized reaction process.[73b] Even so, we would underline that in the long run a fundamental and deep knowledge of what occurs at the active sites will be a necessity for the future, as it will allow to choose more suitable materials and optimize the synthesis strategies with respect to the reaction conditions. Due to its characteristics, X-ray absorption spectroscopy coupled with the advanced data analysis strategies will therefore continue to play an important role in the investigation of the active Cu sites in Cu-zeolites.

Acknowledgments

The authors would like to thank the staff of the ESRF beamlines, where the XAS results reported in the figures of this review were collected: BM23, BM26 DUBBLE, BM31 SNBL, ID26. We are also indebted to S. Svelle, U. Olsbye, S. Bordiga, G. Berlier, and P. Beato for fruitful discussions. KAL and EB would also like to acknowledge and remember Carlo Lamberti, for his brilliant guidance in the use of XAS.

Bibliography

[1] E. McFarland, *Science* **2012**, *338*, 340.

[2] J. Tollefson, *Nature* **2016**.

[3] a) J. S. Woertink, P. J. Smeets, M. H. Groothaert, M. A. Vance, B. F. Sels, R. A. Schoonheydt, E. I. Solomon, *Proc. Natl. Acad. Sci. USA* **2009**, *106*, 18908; b) M. H. Groothaert, P. J. Smeets, B. F. Sels, P. A. Jacobs, R. A. Schoonheydt, *J. Am. Chem. Soc.* **2005**, *127*, 1394; c) V. L. Sushkevich, D. Palagin, M. Ranocchiari, J. A. van Bokhoven, *Science* **2017**, *356*, 523; d) E. M. Alayon, M. Nachtegaal, M. Ranocchiari, J. A. van Bokhoven, *Chem. Commun.* **2012**, *48*, 404; e) S. Grundner, M. A. Markovits, G. Li, M. Tromp, E. A. Pidko, E. J. Hensen, A. Jentys, M. Sanchez-Sanchez, J. A. Lercher, *Nat. Commun.* **2015**, *6*, 7546; f) P. Tomkins, A. Mansouri, S. E. Bozbag, F. Krumeich, M. B. Park, E. M. Alayon, M. Ranocchiari, J. A. van Bokhoven, *Angew. Chem. Int. Ed.* **2016**, *55*, 5467; g) S. Grundner, W. Luo, M. Sanchez-Sanchez, J. A. Lercher, *Chem. Commun.* **2016**, *52*, 2553; h) M. J. Wulfers, S. Teketel, B. Ipek, R. F. Lobo, *Chem. Commun.* **2015**, *51*, 4447; i) D. K. Pappas, E. Borfecchia, M. Dyballa, I. A. Pankin, K. A. Lomachenko, A. Martini, M. Signorile, S. Teketel, B. Arstad, G. Berlier, C. Lamberti, S. Bordiga, U. Olsbye, K. P. Lillerud, S. Svelle, P. Beato, *J. Am. Chem. Soc.* **2017**, *139*, 14961.

[4] N. Kosinov, C. Liu, E. J. M. Hensen, E. A. Pidko, *Chem. Mater.* **2018**, *30*, 3177.

[5] a) U. Olsbye, S. Svelle, M. Bjørgen, P. Beato, T. V. W. Janssens, F. Joensen, S. Bordiga, K. P. Lillerud, *Angew. Chem. Int. Ed.* **2012**, *51*, 5810; b) S. Teketel, W. Skistad, S. Benard, U. Olsbye, K. P. Lillerud, P. Beato, S. Svelle, *ACS Catal.* **2012**, *2*, 26.

[6] a) Y. K. Chow, N. F. Dummer, J. H. Carter, R. J. Meyer, R. D. Armstrong, C. Williams, G. Shaw, S. Yacob, M. M. Bhasin, D. J. Willock, S. H. Taylor, G. J. Hutchings, *ChemPhysChem* **2018**, *19*, 402; b) C. Hammond, M. M. Forde, M. H. Ab Rahim, A. Thetford, Q. He, R. L. Jenkins, N. Dimitratos, J. A. Lopez-Sanchez, N. F. Dummer, D. M. Murphy, A. F. Carley, S. H. Taylor, D. J. Willock, E. E. Stangland, J. Kang, H. Hagen, C. J. Kiely, G. J. Hutchings, *Angew. Chem. Int. Ed.* **2012**, *51*, 5129; c) C. Hammond, I. Hermans, N. Dimitratos, *ChemCatChem* **2015**, *7*, 434; d) C. Hammond, R. L. Jenkins, N. Dimitratos, J. A. Lopez-Sanchez, M. H. ab Rahim, M. M. Forde, A. Thetford, D. M. Murphy, H. Hagen, E. E. Stangland, J. M. Moulijn, S. H. Taylor, D. J. Willock, G. J. Hutchings, *Chem. Eur. J.* **2012**, *18*, 15735; e) K. Yoshizawa, Y. Shiota, T. Yumura, T. Yamabe, *J. Phys. Chem. B* **2000**, *104*, 734; f) V. I. Sobolev, K. A. Dubkov, O. V. Panna, G. I. Panov, *Catal. Today* **1995**, *24*, 251; g) E. V. Starokon, M. V. Parfenov, S. S. Arzumanov, L. V. Pirutko, A. G. Stepanov, G. I. Panov, *J. Catal.* **2013**, *300*, 47; h) M. L. Bols, S. D. Hallaert, B. E. R. Snyder, J. Devos, D. Plessers, H. M. Rhoda, M. Dusselier, R. A. Schoonheydt, K. Pierloot, E. I. Solomon, B. F. Sels, *J. Am. Chem. Soc.* **2018**, *140*, 12021.

[7] a) N. V. Beznis, A. N. C. van Laak, B. M. Weckhuysen, J. H. Bitter, *Micropor. Mesopor. Mat.* **2011**, *138*, 176; b) M. C. Kung, S. S. Y. Lin, H. H. Kung, *Top. Catal.* **2012**, *55*, 108.

[8] J. Shan, W. Huang, L. Nguyen, Y. Yu, S. Zhang, Y. Li, A. I. Frenkel, F. Tao, *Langmuir* **2014**, *30*, 8558.

[9] J. Shan, M. Li, L. F. Allard, S. Lee, M. Flytzani-Stephanopoulos, *Nature* **2017**, *551*, 605.

[10] a) A. A. Gabrienko, S. S. Arzumanov, M. V. Luzgin, A. G. Stepanov, V. N. Parmon, *J. Phys. Chem. C* **2015**, *119*, 24910; b) A. A. Gabrienko, S. S. Arzumanov, A. V. Toktarev, I. G. Danilova, I. P. Prosvirin, V. V. Kriventsov, V. I. Zaikovskii, D. Freude, A. G. Stepanov, *ACS Catal.* **2017**, *7*, 1818; c) A. Oda, T. Ohkubo, T. Yumura, H. Kobayashi, Y. Kuroda, *Inorg. Chem.* **2019**, *58*, 327.

[11] a) G. I. Panov, V. I. Sobolev, A. S. Kharitonov, *J. Mol. Catal.* **1990**, *61*, 85; b) G. I. Panov, V. I. Sobolev, K. A. Dubkov, V. N. Parmon, N. S. Ovanesyan, A. E. Shilov, A. A. Shteinman, *React. Kinet. Catal. Lett.* **1997**, *61*, 251.

[12] a) B. E. R. Snyder, M. L. Bols, R. A. Schoonheydt, B. F. Sels, E. I. Solomon, *Chem. Rev.* **2018**, *118*, 2718; b) B. E. Snyder, P. Vanelderen, M. L. Bols, S. D. Hallaert, L. H. Bottger, L. Ungur, K. Pierloot, R. A. Schoonheydt, B. F. Sels, E. I. Solomon, *Nature* **2016**, *536*, 317.

[13] J. Xu, R. D. Armstrong, G. Shaw, N. F. Dummer, S. J. Freakley, S. H. Taylor, G. J. Hutchings, *Catal. Today* **2016**, *270*, 93.

[14] G. J. Hutchings, *Top. Catal.* **2016**, *59*, 658.

[15] a) N. V. Beznis, B. M. Weckhuysen, J. H. Bitter, *Catal. Lett.* **2010**, *136*, 52; b) D. Kaucky, J. I. Dědeček, B. Wichterlová, *Micropor. Mesopor. Mat.* **1999**, *31*, 75; c) K. Nakamura, A. Okuda, K. Ohta, H. Matsubara, K. Okumura, K. Yamamoto, R. Itagaki, S. Suganuma, E. Tsuji, N. Katada, *ChemCatChem* **2018**, *10*, 3806.

[16] a) A. G. Stepanov, S. S. Arzumanov, A. A. Gabrienko, V. N. Parmon, I. I. Ivanova, D. Freude, *ChemPhysChem* **2008**, *9*, 2559; b) A. G. Stepanov, S. S. Arzumanov, A. A. Gabrienko, A. V. Toktarev, V. N. Parmon, D. Freude, *J. Catal.* **2008**, *253*, 11.

[17] S. H. Lee, J. K. Kang, E. D. Park, *Korean J. Chem. Eng.* **2018**, *35*, 2145.

[18] E. V. Kondratenko, T. Peppel, D. Seeburg, V. A. Kondratenko, N. Kalevaru, A. Martin, S. Wohlrab, *Catal. Sci. Technol.* **2017**, *7*, 366.

[19] a) S. Sato, Y. Yoshihiro, H. Yahiro, N. Mizuno, M. Iwamoto, *Appl. Catal.* **1991**, *70*, L1; b) M. Iwamoto, *Stud. Surf. Sci. Catal.* **1991**, *60*, 327; c) M. Iwamoto, S. Yokoo, K. Sakai, S. Kagawa, *J. Chem. Soc. Faraday Trans.* **1981**, *77*, 1629.

[20] a) M. H. Groothaert, K. Lievens, H. Leeman, B. M. Weckhuysen, R. A. Schoonheydt, *J. Catal.* **2003**, *220*, 500; b) M. H. Groothaert, K. Lievens, J. A. van Bokhoven, A. A. Battiston, B. M. Weckhuysen, K. Pierloot, R. A. Schoonheydt, *ChemPhysChem* **2003**, *4*, 626; c) M. V. Konduru, S. S. C. Chuang, *J. Catal.* **2000**, *196*, 271; d) P. J. Smeets, M. H. Groothaert, R. M. van Teeffelen, H. Leeman, E. J. M. Hensen, R. A. Schoonheydt, *J. Catal.* **2007**, *245*, 358; e) B. Wichterlová, J. Dědeček, Z. Sobalík, A. Vondrova, K. Klier, *J. Catal.* **1997**, *169*, 194.

[21] a) M. Koebel, M. Elsener, M. Kleemann, *Catal. Today* **2000**, *59*, 335; b) Z. Schay, L. Guczi, A. Beck, I. Nagy, V. Samuel, S. P. Mirajkar, A. V. Ramaswamy, G. Pál-Borbély, *Catal. Today* **2002**, *75*, 393; c) C. Paolucci, J. R. Di Iorio, F. H. Ribeiro, R. Gounder, W. F. Schneider, *Adv. Catal.* **2016**, *59*, 1.

[22] M. Shelef, *Chem. Rev.* **1995**, *95*, 209.

[23] a) C. Paolucci, A. A. Parekh, I. Khurana, J. R. Di Iorio, H. Li, J. D. Albarracin Caballero, A. J. Shih, T. Anggara, W. N. Delgass, J. T. Miller, F. H. Ribeiro, R. Gounder, W. F. Schneider, *J. Am. Chem. Soc.* **2016**, *138*, 6028; b) K. A. Lomachenko, E. Borfecchia, S. Bordiga, A. V. Soldatov, P. Beato, C. Lamberti, *J. Phys.: Conf. Ser.* **2016**, *712*, 012041; c) J. H. Kwak, R. G. Tonkyn, D. H. Kim, J. Szanyi, C. H. F. Peden, *J. Catal.* **2010**, *275*, 187; d) J. H. Kwak, J. H. Lee, D. Tran, R. R. Tonkyn, J. Szanyi, C. H. F. Peden, *Abstr. Pap. Am. Chem. Soc.* **2011**, *242*, 1; e) U. Deka, A. Juhin, E. A. Eilertsen, H. Emerich, M. A. Green, S. T. Korhonen, B. M. Weckhuysen, A. M. Beale, *J. Phys. Chem. C* **2012**, *116*, 4809; f) J. H. Kwak, H. Y. Zhu, J. H. Lee, C. H. F. Peden, J. Szanyi, *Chem. Commun.* **2012**, *48*, 4758; g) J. S. McEwen, T. Anggara, W. F. Schneider, V. F. Kispersky, J. T. Miller, W. N. Delgass, F. H. Ribeiro, *Catal. Today* **2012**, *184*, 129; h) F. Gao, E. D. Walter, E. M. Karp, J. Luo, R. G. Tonkyn, J. H. Kwak, J. Szanyi, C. H. F. Peden, *J. Catal.* **2013**, *300*, 20; i) F. Giordanino, P. N. R. Vennestrom, L. F. Lundegaard, F. N. Stappen, S. Mossin, P. Beato, S.

Bordiga, C. Lamberti, *Dalton Trans.* **2013**, *42*, 12741; j) F. Göltl, R. E. Bulo, J. Hafner, P. Sautet, *J. Phys. Chem. Lett.* **2013**, *4*, 2244; k) F. Gao, E. D. Walter, M. Kollar, Y. Wang, J. Szanyi, C. H. F. Peden, *J. Catal.* **2014**, *319*, 1; l) F. Giordanino, E. Borfecchia, K. A. Lomachenko, A. Lazzarini, G. Agostini, E. Gallo, A. V. Soldatov, P. Beato, S. Bordiga, C. Lamberti, *J. Phys. Chem. Lett.* **2014**, *5*, 1552; m) J. H. Kwak, T. Varga, C. H. F. Peden, F. Gao, J. C. Hanson, J. Szanyi, *J. Catal.* **2014**, *314*, 83; n) C. Paolucci, A. A. Verma, S. A. Bates, V. F. Kispersky, J. T. Miller, R. Gounder, W. N. Delgass, F. H. Ribeiro, W. F. Schneider, *Angew. Chem. Int. Ed.* **2014**, *53*, 11828; o) E. Borfecchia, K. A. Lomachenko, F. Giordanino, H. Falsig, P. Beato, A. V. Soldatov, S. Bordiga, C. Lamberti, *Chem. Sci.* **2015**, *6*, 548; p) F. Gao, Y. Wang, N. M. Washton, M. Kollár, J. Szanyi, C. H. F. Peden, *ACS Catal.* **2015**, *5*, 6780; q) F. Gao, N. M. Washton, Y. L. Wang, M. Kollar, J. Szanyi, C. H. F. Peden, *J. Catal.* **2015**, *331*, 25; r) T. Gunter, H. W. P. Carvalho, D. E. Doronkin, T. Sheppard, P. Glatzel, A. J. Atkins, J. Rudolph, C. R. Jacob, M. Casapu, J. D. Grunwaldt, *Chem. Commun.* **2015**, *51*, 9227; s) A. M. Beale, I. Lezcano-Gonzalez, W. A. Slawinksi, D. S. Wragg, *Chem. Commun.* **2016**, *52*, 6170; t) F. Göltl, P. Sautet, I. Hermans, *Catal. Today* **2016**, *267*, 41; u) C. Paolucci, I. Khurana, A. A. Parekh, S. Li, A. J. Shih, H. Li, J. R. Di Iorio, J. D. Albarracin-Caballero, A. Yezerets, J. T. Miller, W. N. Delgass, F. H. Ribeiro, W. F. Schneider, R. Gounder, *Science* **2017**, *357*, 898; v) T. V. W. Janssens, H. Falsig, L. F. Lundegaard, P. N. R. Vennestrøm, S. B. Rasmussen, P. G. Moses, F. Giordanino, E. Borfecchia, K. A. Lomachenko, C. Lamberti, S. Bordiga, A. Godiksen, S. Mossin, P. Beato, *ACS Catal.* **2015**, *5*, 2832; w) C. Tyrsted, E. Borfecchia, G. Berlier, K. A. Lomachenko, C. Lamberti, S. Bordiga, P. N. R. Vennestrøm, T. V. W. Janssens, H. Falsig, P. Beato, A. Puig-Molina, *Catal. Sci. Technol.* **2016**, *6*, 8314.

[24] a) H. Yamanaka, R. Hamada, H. Nibuta, S. Nishiyama, S. Tsuruya, *J. Mol. Catal. A Chem.* **2002**, *178*, 89; b) R. Hamada, Y. Shibata, S. Nishiyama, S. Tsuruya, *Phys. Chem. Chem. Phys.* **2003**, *5*, 956; c) A. Tabler, A. Häusser, E. Roduner, *J. Mol. Catal. A Chem.* **2013**, *379*, 139; d) A. Kubacka, Z. Wang, B. Sulikowski, V. Cortés Corberán, *J. Catal.* **2007**, *250*, 184.

[25] a) P. Vanelderen, J. Vancauwenbergh, B. F. Sels, R. A. Schoonheydt, *Coord. Chem. Rev.* **2013**, *257*, 483; b) G. Brezicki, J. D. Kammert, T. B. Gunnoe, C. Paolucci, R. J. Davis, *ACS Catal.* **2019**, *9*, 5308.

[26] D. W. Fickel, J. M. Fedeyko, R. F. Lobo, *J. Phys. Chem. C* **2010**, *114*, 1633.

[27] a) A. Martini, E. Borfecchia, K. A. Lomachenko, I. A. Pankin, C. Negri, G. Berlier, P. Beato, H. Falsig, S. Bordiga, C. Lamberti, *Chem. Sci.* **2017**, *8*, 6836; b) C. W. Andersen, M. Bremholm, P. N. R. Vennestrom, A. B. Blichfeld, L. F. Lundegaard, B. B. Iversen, *IUCrJ* **2014**, *1*, 382.

[28] B. Ipek, M. J. Wulfers, H. Kim, F. Göltl, I. Hermans, J. P. Smith, K. S. Booksh, C. M. Brown, R. F. Lobo, *ACS Catal.* **2017**, *7*, 4291.

[29] a) J. Dědeček, B. Wichterlová, *J. Phys. Chem. B* **1999**, *103*, 1462; b) R. Bulánek, K. Frolich, P. Cicmanec, D. Nachtigallová, A. Pulido, P. Nachtigall, *J. Phys. Chem. C* **2011**, *115*, 13312; c) R. Bulánek, B. Wichterlová, Z. Sobalík, J. Tichý, *Appl. Catal. B Environ.* **2001**, *31*, 13; d) P. Nachtigall, R. Bulánek, *Appl. Catal. A Gen.* **2006**, *307*, 118.

[30] M. P. Attfield, S. J. Weigel, A. K. Cheetham, *J. Catal.* **1997**, *172*, 274.

[31] S. D. Hallaert, M. L. Bols, P. Vanelderen, R. A. Schoonheydt, B. F. Sels, K. Pierloot, *Inorg. Chem.* **2017**, *56*, 10681.

[32] S. Sklenak, P. C. Andrikopoulos, S. R. Whittleton, H. Jirglova, P. Sazama, L. Benco, T. Bucko, J. Hafner, Z. Sobalik, *J. Phys. Chem. C* **2013**, *117*, 3958.

[33] Y. Kuroda, A. Kotani, H. Maeda, H. Moriwaki, T. Morimato, M. Nagao, *J. Chem. Soc. Faraday Trans.* **1992**, *88*, 1583.

[34] P. Vanelderen, J. Vancauwenbergh, M.-L. Tsai, R. G. Hadt, E. I. Solomon, R. A. Schoonheydt, B. F. Sels, *ChemPhysChem* **2014**, *15*, 91.

[35] P. Vanelderen, B. E. Snyder, M. L. Tsai, R. G. Hadt, J. Vancauwenbergh, O. Coussens, R. A. Schoonheydt, B. F. Sels, E. I. Solomon, *J. Am. Chem. Soc.* **2015**, *137*, 6383.

[36] B. E. R. Snyder, P. Vanelderen, R. A. Schoonheydt, B. F. Sels, E. I. Solomon, *J. Am. Chem. Soc.* **2018**, *140*, 9236.

[37] A. Julbe, M. Drobek, in *Encyclopedia of Membranes* (Eds.: E. Drioli, L. Giorno), Springer Berlin Heidelberg, Berlin, Heidelberg, **2015**.

[38] A. Dyer, in *Encyclopedia of Materials: Science and Technology*, Elsevier Science Ltd., **2001**, pp. 9859.

[39] J. V. Smith, *Adv. Chem.* **1974**, *101*, 171.

[40] S. Santra, T. Archipov, A. B. Ene, H. Komnik, H. Stoll, E. Roduner, G. Rauhut, *Phys. Chem. Chem. Phys.* **2009**, *11*, 8855.

[41] A. Dyer, *An Introduction to Zeolite Molecular Sieves*, John Wiley & Sons, **1988**.

[42] I. E. Maxwell, J. J. d. Boer, *J. Phys. Chem.* **1975**, *79*, 1874.

[43] P. J. Smeets, J. S. Woertink, B. F. Sels, E. I. Solomon, R. A. Schoonheydt, *Inorg. Chem.* **2010**, *49*, 3573.

[44] G. D. E. A. Villagomez, J.-M. Ducere, D. Berthomieu, A. Goursot, B. Coq, *ChemPhysChem* **2002**, *3*, 686.

[45] A. M. Goossens, E. J. P. Feijen, G. Verhoeven, B. H. Wouters, P. J. Grobet, P. A. Jacobs, J. A. Martens, *Micropor. Mesopor. Mat.* **2000**, *35-36*, 555.

[46] J.-S. Yu, J. Y. Kim, *Catal. Today* **1998**, *44*, 81.

[47] J. F. Cole, H. W. Kouwenhoven, *Adv. Chem.* **1973**, *121*, 583.

[48] A. Martucci, A. Alberti, M. de Lourdes Guzman-Castillo, F. Di Renzo, F. Fajula, *Micropor. Mesopor. Mat.* **2003**, *63*, 33.

[49] P. Rejmak, J. Datka, E. Broclawik, *Int. J. Quantum Chem.* **2018**, *119*.

[50] P. Massiani, F. Fajula, F. Figueras, J. Sanz, *Zeolites* **1988**, *8*, 332.

[51] N. V. Beznis, B. M. Weckhuysen, J. H. Bitter, *Catal. Lett.* **2010**, *138*, 14.

[52] P. J. Smeets, M. H. Groothaert, R. A. Schoonheydt, *Catal. Today* **2005**, *110*, 303.

[53] a) E. M. C. Alayon, M. Nachtegaal, A. Bodi, M. Ranocchiari, J. A. van Bokhoven, *Phys. Chem. Chem. Phys.* **2015**, *17*, 7681; b) E. M. C. Alayon, M. Nachtegaal, A. Bodi, J. A. van Bokhoven, *ACS Catal.* **2014**, *4*, 16; c) V. L. Sushkevich, D. Palagin, J. A. van Bokhoven, *Angew. Chem. Int. Ed.* **2018**, *57*, 8906; d) V. L. Sushkevich, J. A. van Bokhoven, *Catal. Sci. Technol.* **2018**, *8*, 4141; e) M. B. Park, S. H. Ahn, A. Mansouri, M. Ranocchiari, J. A. van Bokhoven, *ChemCatChem* **2017**, *9*, 3705; f) E. Borfecchia, D. K. Pappas, M. Dyballa, K. A. Lomachenko, C. Negri, M. Signorile, G. Berlier, *Catal. Today* **2019**, *333*, 17; g) D. K. Pappas, A. Martini, M. Dyballa, K. Kvande, S. Teketel, K. A. Lomachenko, R. Baran, P. Glatzel, B. Arstad, G. Berlier, C. Lamberti, S. Bordiga, U. Olsbye, S. Svelle, P. Beato, E. Borfecchia, *J. Am. Chem. Soc.* **2018**, *140*, 15270; h) M. Dyballa, D. K. Pappas, K. Kvande, E. Borfecchia, B. Arstad, P. Beato, U. Olsbye, S. Svelle, *ACS Catal.* **2019**, *9*, 365; i) H. V. Le, S. Parishan, A. Sagaltchik, C. Göbel, C. Schlesiger, W. Malzer, A. Trunschke, R. Schomäcker, A. Thomas, *ACS Catal.* **2017**, *7*, 1403; j) T. Ikuno, S. Grundner, A. Jentys, G. Li, E. Pidko, J. Fulton, M. Sanchez-Sanchez, J. A. Lercher, *J. Phys. Chem. C* **2019**, *123*, 8759.

[54] a) T. Sheppard, C. D. Hamill, A. Goguet, D. W. Rooney, J. M. Thompson, *Chem. Commun.* **2014**, *50*, 11053; b) P. Vanelderen, R. G. Hadt, P. J. Smeets, E. I. Solomon, R. A. Schoonheydt, B. F. Sels, *J. Catal.* **2011**, *284*, 157; c) P. Vanelderen, P. J. Smeets, R. G. Hadt, J. S. Woertink, R. A. Schoonheydt, B. F. Sels, E. I. Solomon, *Abstr. Pap. Am. Chem. Soc.* **2011**, *242*; d) M. A. C. Markovits, A. Jentys, M. Tromp, M. Sanchez-Sanchez, J. A. Lercher, *Top. Catal.* **2016**, *59*, 1554; e) K. Narsimhan, K. Iyoki, K. Dinh, Y. Roman-Leshkov, *ACS Cent. Sci.* **2016**, *2*, 424.

[55] a) B. Ipek, R. F. Lobo, *Chem. Commun.* **2016**, *52*, 13401; b) R. Oord, J. E. Schmidt, B. M. Weckhuysen, *Catal. Sci. Technol.* **2018**, *8*, 1028; c) E. Borfecchia, P. Beato, S. Svelle, U. Olsbye, C. Lamberti, S. Bordiga, *Chem. Soc. Rev.* **2018**.

[56] A. J. Knorpp, A. B. Pinar, M. A. Newton, V. L. Sushkevich, J. A. van Bokhoven, *ChemCatChem* **2018**, *10*, 5593.

[57] H. V. Le, S. Parishan, A. Sagaltchik, H. Ahi, A. Trunschke, R. Schomäcker, A. Thomas, *Chem. Eur. J.* **2018**, *24*, 12592.

[58] S. E. Bozbag, P. Sot, M. Nachtegaal, M. Ranocchiari, J. A. van Bokhoven, C. Mesters, *ACS Catal.* **2018**, *8*, 5721.

[59] J. Meyet, K. Searles, M. A. Newton, M. Wörle, A. P. van Bavel, A. D. Horton, J. A. van Bokhoven, C. Copéret, *Angew. Chem. Int. Ed.* **2019**, *58*, 9841.

[60] Y. Kim, T. Y. Kim, H. Lee, J. Yi, *Chem. Commun.* **2017**, *53*, 4116.

[61] X. Wang, N. M. Martin, J. Nilsson, S. Carlson, J. Gustafson, M. Skoglundh, P.-A. Carlsson, *Catalysts* **2018**, *8*, 545.

[62] M. H. Mahyuddin, Y. Shiota, K. Yoshizawa, *Catal. Sci. Technol.* **2019**, *9*, 1744.

[63] A. J. Knorpp, M. A. Newton, A. B. Pinar, J. A. van Bokhoven, *Ind. Eng. Chem. Res.* **2018**, *57*, 12036.

[64] P. J. Smeets, M. H. Groothaert, R. A. Schoonheydt, *Catal. Today* **2005**, *110*, 303.

[65] M. H. Mahyuddin, Y. Shiota, A. Staykov, K. Yoshizawa, *Acc. Chem. Res.* **2018**, *51*, 2382.

[66] a) M. H. Mahyuddin, A. Staykov, Y. Shiota, M. Miyanishi, K. Yoshizawa, *ACS Catal.* **2017**, *7*, 3741; b) Z.-J. Zhao, A. Kulkarni, L. Vilella, J. K. Nørskov, F. Studt, *ACS Catal.* **2016**, *6*, 3760; c) M. H. Mahyuddin, T. Tanaka, Y. Shiota, A. Staykov, K. Yoshizawa, *ACS Catal.* **2018**, *8*, 1500.

[67] P. Tomkins, M. Ranocchiari, J. A. van Bokhoven, *Acc. Chem. Res.* **2017**, *50*, 418.

[68] V. L. Sushkevich, J. A. van Bokhoven, *ACS Catal.* **2019**, *9*, 6293.

[69] J.-P. Lange, V. L. Sushkevich, A. J. Knorpp, J. A. van Bokhoven, *Ind. Eng. Chem. Res.* **2019**, *58*, 8674.

[70] A. R. Kulkarni, Z.-J. Zhao, S. Siahrostami, J. K. Nørskov, F. Studt, *Catal. Sci. Technol.* **2018**, *8*, 114.

[71] S. E. Bozbag, E. M. C. Alayon, J. Pecháček, M. Nachtegaal, M. Ranocchiari, J. A. van Bokhoven, *Catal. Sci. Technol.* **2016**, *6*, 5011.

[72] A. R. Kulkarni, Z.-J. Zhao, S. Siahrostami, J. K. Nørskov, F. Studt, *ACS Catal.* **2016**, *6*, 6531.

[73] a) M. Ravi, M. Ranocchiari, J. A. van Bokhoven, *Angew. Chem. Int. Ed.* **2017**, *56*, 16464; b) M. Ravi, V. L. Sushkevich, A. J. Knorpp, M. A. Newton, D. Palagin, A. B. Pinar, M. Ranocchiari, J. A. van Bokhoven, *Nat. Catal.* **2019**, *2*, 485.

[74] S. Bordiga, C. Lamberti, F. Bonino, A. Travert, F. Thibault-Starzyk, *Chem. Soc. Rev.* **2015**, *44*, 7262.

[75] a) S. Bordiga, E. Groppo, G. Agostini, J. A. van Bokhoven, C. Lamberti, *Chem. Rev.* **2013**, *113*, 1736; b) K. A. Lomachenko, E. Borfecchia, C. Negri, G. Berlier, C. Lamberti, P. Beato, H. Falsig, S. Bordiga, *J. Am. Chem. Soc.* **2016**, *138*, 12025−12028.

[76] a) E. R. Malinowski, *Factor analysis in chemistry*, Wiley, **2002**; b) C. Ruckebusch, L. Blanchet, *Anal. Chim. Acta* **2013**, *765*, 28; c) R. Tauler, *Chemometr. Intell. Lab.* **1995**, *30*, 133; d) A. de Juan, R. Tauler, *Anal. Chim. Acta* **2003**, *500*, 195.

[77] a) J. Jaumot, A. de Juan, R. Tauler, *Chemometr. Intell. Lab.* **2015**, *140*, 1; b) J. Jaumot, R. Gargallo, A. de Juan, R. Tauler, *Chemometr. Intell. Lab.* **2005**, *76*, 101; c) C. Ruckebusch, *Resolving Spectral Mixtures: With Applications from Ultrafast Time-Resolved Spectroscopy to Super-Resolution Imaging, Vol. 30*, Elsevier, **2016**.

[78] A. Voronov, A. Urakawa, W. v. Beek, N. E. Tsakoumis, H. Emerich, M. Rønning, *Anal. Chim. Acta* **2014**, *840*, 20.

[79] E. I. Solomon, D. E. Heppner, E. M. Johnston, J. W. Ginsbach, J. Cirera, M. Qayyum, M. T. Kieber-Emmons, C. H. Kjaergaard, R. G. Hadt, L. Tian, *Chem. Rev.* **2014**, *114*, 3659.

[80] V. L. Sushkevich, A. V. Smirnov, J. A. van Bokhoven, *J. Phys. Chem. C* **2019**, *123*, 9926.

[81] A. Martini, E. Alladio, E. Borfecchia, *Top. Catal.* **2018**, *61*, 1396.

[82] E. A. Pidko, E. J. M. Hensen, R. A. van Santen, *Proc. R. Soc. A-Math. Phys. Eng. Sci.* **2012**, *468*, 2070.

[83] L. Artiglia, V. L. Sushkevich, D. Palagin, A. J. Knorpp, K. Roy, J. A. van Bokhoven, *ACS Catal.* **2019**, *9*, 6728.

[84] M. Dyballa, K. Thorshaug, D. K. Pappas, E. Borfecchia, K. Kvande, S. Bordiga, G. Berlier, A. Lazzarini, U. Olsbye, P. Beato, S. Svelle, B. Arstad, *ChemCatChem* **2019**, *11*, 5022.

[85] V. L. Sushkevich, R. Verel, J. A. van Bokhoven, *Angew. Chem. Int. Ed.* **2019**, *132*, 920.

[86] P. J. Smeets, R. G. Hadt, J. S. Woertink, P. Vanelderen, R. A. Schoonheydt, B. F. Sels, E. I. Solomon, *J. Am. Chem. Soc.* **2010**, *132*, 14736.

[87] G. Li, P. Vassilev, M. Sanchez-Sanchez, J. A. Lercher, E. J. M. Hensen, E. A. Pidko, *J. Catal.* **2016**, *338*, 305.

[88] M. A. Newton, A. J. Knorpp, A. B. Pinar, V. L. Sushkevich, D. Palagin, J. A. van Bokhoven, *J. Am. Chem. Soc.* **2018**, *140*, 10090.

[89] T. Yumura, Y. Hirose, T. Wakasugi, Y. Kuroda, H. Kobayashi, *ACS Catal.* **2016**, *6*, 2687.

[90] K. A. Lomachenko, A. Martini, D. K. Pappas, C. Negri, M. Dyballa, G. Berlier, S. Bordiga, C. Lamberti, U. Olsbye, S. Svelle, P. Beato, E. Borfecchia, *Catal. Today* **2019**, *336*, 99.